Degree-of-Freedom Gain From Using Polarimetric Antenna Elements

Ada S. Y. Poon, *Senior Member, IEEE*, and David N. C. Tse, *Fellow, IEEE*

***Abstract*—Polarization could be the last resource to be exploited for space-limited devices. Over the past years, theoretical studies and experimental work present different conclusions on the potential increase in the number of degrees of freedom from polarization. This paper attempts to unify the different conclusions and provide a mathematical framework that can be applied to any array geometry and channel scattering condition. It shows that the degree-of-freedom gain from using polarimetric antenna elements ranges from 2 to 6 and the gain depends on the array geometry and the channel scattering condition. Sampling techniques and vector multipole decomposition are applied to derive the results.**

***Index Terms*—Degrees of freedom, multiple antennas, multiple-input multiple-output (MIMO) systems, physical channel modeling, polarization.**

I. Introduction

THE extra degrees of freedom from polarization effectively increase the number of communication channels between transceivers without increasing the space occupied by the transceiver arrays. Exploitation of polarization in wireless systems therefore represents a formidable opportunity, particularly for space-constrained base-stations and mobiles. Over the past years, theoretical studies and experimental work present different conclusions on the potential increase in the number of degrees of freedom from polarization. Andrews *et al.* [1] demonstrated experimentally that three co-located orthogonal electric dipoles attains 3 degrees of freedom. Svantesson *et al.* [2] showed analytically that six co-located orthogonal electric dipoles and orthogonal magnetic dipoles (a polarimetric antenna element) attain 6 degrees of freedom. Gustafsson *et al.* [3] illustrated that six electric dipoles centered on the edges of a tetrahedron of length 0.3 wavelength attains 6 degrees of freedom. As a result, it is speculated that there is 6-fold increase in the degrees of freedom from an array of polarimetric antenna elements. On the other hand, Marzetta [4] stated that there is 4-fold increase in the degrees of freedom. Our earlier paper [5] claimed that there is only 2-fold increase and scatterers would not increase the degrees of freedom from the use of polarimetric antenna elements. From Physics, the six components of electric and magnetic field emanate from a source region are not independent. Two scalar equations are sufficient to capture the electrodynamic phenomenon [6, Ch. 1]. This suggests that there is only 2-fold increase in the degrees of freedom from polarization no matter whether there is scatterer or not.

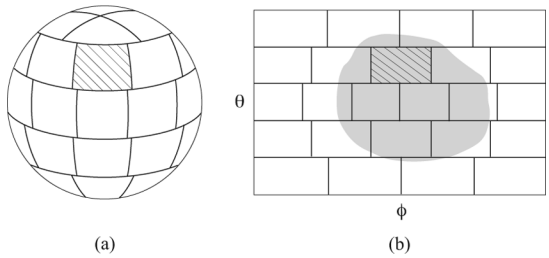

Fig. 1. Illustrates the set of resolvable angular cells by a spherical array.

While the reported results hold and do not violate physical laws, they are true only under certain geometry of antenna arrays and scattering condition of channels. This paper attempts to unify the different conclusions and provides a mathematical framework that can be applied to any array geometry and channel scattering condition. Let us first outline our steps of reasoning:

1) Resolvable angular cells. Any antenna array attains certain radiation pattern—the directional (angular) dependence of the field emanated from the array at a distance. This radiation pattern is confined to certain angular region. For example, a spherical array is able to generate radiation pattern confined to the angular cells shown in Fig. 1(a). The patterned region is one of the resolvable angular cells. For ease of drawing, we unroll the cells and show them on a 2-D plane by their elevation (θ) and azimuth (ϕ) angles as shown in Fig. 1(b).
2) Array degree-of-freedom. In a scattering environment, certain directions of the radiating field will be diffracted or reflected by scatterers. These directions correspond to the directions of departure (DOD) of physical paths. The number of angular cells that overlap with these directions yields the dimension of the transmit signal space in the spatial domain. For example, the shaded region in Fig. 1(b) corresponds to the set of DOD. Signals radiated in the shaded region could possibly reach the receiver. Similarly, the number of angular cells that overlap with the directions of arrival of physical paths at the receiver yields the dimension of the receive signal space. The minimum of the number of overlapped angular cells at the transmitter and

Manuscript received April 23, 2009; revised April 14, 2011; accepted April 14, 2011. Date of current version August 31, 2011. The material in this paper was presented in part at the IEEE International Symposium on Information Theory, Toronto, ON, July 2008.

A. S. Y. Poon is with the Department of Electrical Engineering, Stanford University, CA 94305 USA (e-mail: adapoon@stanford.edu).

D. N. C. Tse is with the Department of Electrical Engineering and Computer Sciences, University of California, Berkeley, CA 94704 USA (e-mail: dtse@eecs.berkeley.edu).

Communicated by L. Zheng, Associate Editor for Communications.

Color versions of one or more of the figures in this paper are available online at http://ieeexplore.ieee.org.

Digital Object Identifier 10.1109/TIT.2011.2161952

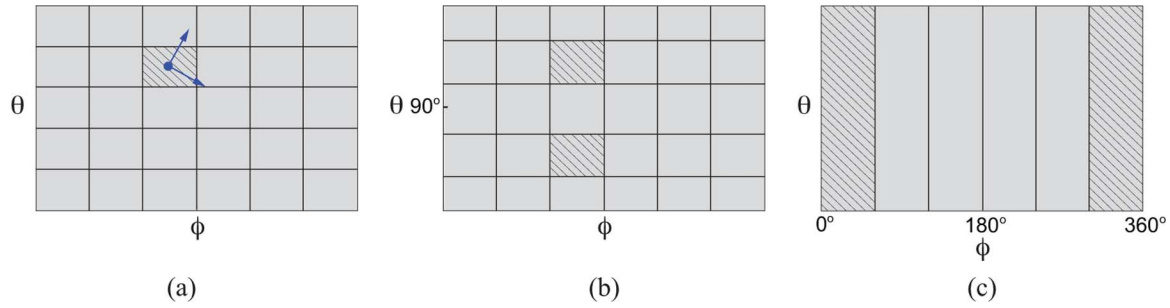

Fig. 2. Sketches the angular resolvable cells for three different dimensions of array geometry and illustrates the degree-of-freedom gain in a fully-scattered environment. (a) Volumetric array. (b) Planar array lying on the xy-plane, $\theta = 90°$. (c) Linear array along the x-axis, $\phi = 0°$.

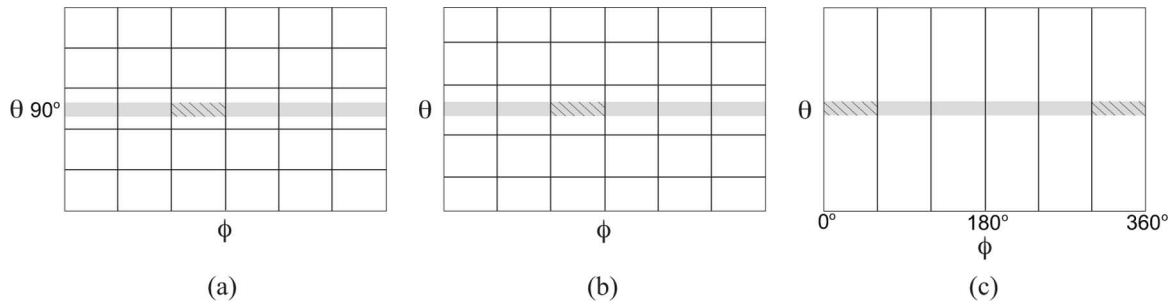

Fig. 3. Illustrates the degree-of-freedom gain in an azimuth-scattered environment. (a) Volumetric array. (b) Planar array lying on the xy-plane, $\theta = 90°$. (c) Linear array along the x-axis, $\phi = 0°$.

that at the receiver yields the number of spatial degrees of freedom from using uni-polarized antenna elements.

3) Polarization degree-of-freedom. When uni-polarized antenna elements are used, each pair of overlapped cell at the transmitter and that at the receiver can be modeled by a complex gain. When polarimetric antenna elements are used, the complex gain becomes a 6×6 complex matrix. The rank of this complex matrix yields the degree-of-freedom gain from using polarimetric antenna elements. The total number of spatial degrees of freedom is the product of the array degree-of-freedom and the polarization degree-of-freedom.

Given an unambiguous definition of the degree-of-freedom gain, we will consider the gain for linear, planar, and volumetric arrays in fully-scattered and azimuth-scattered environments.

In a fully-scattered environment, the shaded region is the entire (θ, ϕ)-plane. A volumetric array such as a spherical array is able to resolve both θ and ϕ directions, and the resolvable cells are shown in Fig. 2(a). In each resolvable cell, polarimetric antenna elements can be used to resolve the direction of electromagnetic fields, which is perpendicular to their direction of propagation and is tangential to the resolvable angular cells. The field direction in one of the resolvable cells is therefore spanned by the two vectors shown in Fig. 2(a). Hence, the degree-of-freedom gain from using polarimetric antenna elements is 2. A planar array lying on the xy-plane $(\theta = 90°)$ is also able to resolve both θ and ϕ directions. But it cannot distinguish physical path coming from above or below the array; that is, the two patterned regions in Fig. 2(b) belong to the same resolvable angular cell. Polarimetric antenna elements can resolve not only the field directions but also the propagation direction of physical paths coming from (θ, ϕ) versus $(\pi - \theta, \phi)$. Hence, the degree-of-freedom gain is doubled and equals to 4. On the other hand, a linear array lying along the x-axis can resolve the ϕ direction only. But it cannot distinguish physical path coming from ϕ versus $2\pi - \phi$; that is, the two patterned strips in Fig. 2(c) belong to the same resolvable angular cell. Polarimetric antenna elements can resolve not only the field directions but also the propagation direction of physical paths along θ. The degree-of-freedom gain therefore equals to the number of co-located orthogonal dipoles which is 6.

In an azimuth-scattered environment, the direction of physical paths clusters around $\theta = 90°$–the shaded strips in Fig. 3. For volumetric arrays, the resolvable cells that overlap with the shaded strip, attain 2 degrees of freedom from resolving the field directions. For planar arrays, the resolvable cells are connected. We would not get the extra factor of two from resolving physical paths coming from $\theta > 90°$ versus $\theta < 90°$. The degree-of-freedom gain remains 2. For linear arrays, the resolvable cells are disconnected and are partitioned into $\mathcal{S}$ and $2\pi - \mathcal{S}$ where $\mathcal{S}$ is connected. Polarimetric antenna elements can resolve the two disconnected regions which is equivalent to resolving physical paths coming from ϕ versus $2\pi - \phi$. Therefore, the number of degrees of freedom is doubled and equals to 4.

Table I summarizes our main results. Inevitably, there are only two degrees of freedom from resolving the direction of electromagnetic fields by polarimetric antenna elements. The extra multiplicative gain in some array geometries is due to the use of polarimetric antenna elements in resolving the propagation directions of physical paths. In particular, lower dimensional array geometries are less effective in resolving the direction of physical paths. Hence, they have higher degree-of-freedom gain from using polarimetric antenna elements. Strictly speaking, the degree-of-freedom gain from resolving the direc-

TABLE I
MULTIPLICATIVE GAIN IN DEGREES OF FREEDOM FROM USING POLARIMETRIC ANTENNA ELEMENTS

Channel	Array Geometries			
	Point	Linear	Planar	Volumetric
Fully-Scattered	6	6	4	2
Azimuth-Scattered	6	4	2	2

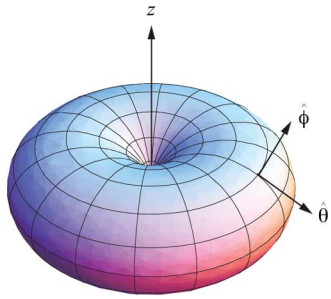

Fig. 4. Radiation pattern of an electric and a magnetic dipole oriented along the z-axis.

tion of electromagnetic fields should be considered as the polarization degrees of freedom which are 2 in all cases and agree with physical laws.

The resolvable angular cells in Figs. 2 and 3 give a contrast among different array geometries but they do not correspond to the actual shape of the resolvable cells. To obtain the set of resolvable cells, we will use a *sampling* approach. Any geometry of antenna array has a certain range of resolvable propagation directions. For example, a linear array can resolve $0 \leq \phi < \pi$ as shown in Fig. 2(c). This resolvable angular range is analogous to the spectral bandwidth of a time-domain signal. On knowing the signal bandwidth, we obtain the optimal sampling period in the time domain. Similarly, on knowing the resolvable angular range, we will obtain the optimal placement of antenna elements on the array. This optimal placement, in turn, will reveal the set of resolvable angular cells. For completeness, we will also introduce a physical approach based on the *multipole decomposition* of vector fields to derive the degree-of-freedom gain.

The rest of the paper is organized as follows. Section II presents the complex matrix that models the correlation between a pair of polarimetric antenna elements, and investigates the degree-of-freedom gain and diversity gain in both fully-scattered and azimuth-scattered environments. Sections III–V extend the model and studies to arrays of polarimetric antenna elements in various array geometries. Section VI presents an alternate approach based on vector multipole decomposition. Finally, we will conclude this paper in Section VII.

The following notation will be used in this paper. We will use boldface capital letters for matrices $(\mathbf{C}, \mathbf{H}, \ldots)$, boldface lower case letters for vectors $(\mathbf{p}, \mathbf{q}, \ldots)$, and calligraphic boldface capital letters for electromagnetic entities $(\boldsymbol{\mathcal{E}})$. For a given vector $\mathbf{r}$, $\hat{\mathbf{r}}$ is a unit vector denoting its direction and r denotes its magnitude. $\mathbf{I}$ is the identity matrix. $(\cdot)^*$, $(\cdot)^\dagger$ and $\mathsf{E}[\cdot]$ denote conjugate, conjugate-transpose and expectation operations respectively.

II. POINT SOURCES

Point source refers to the six co-located orthogonal dipoles. In this section, we will model the response between a transmit and a receive point source, and derive the degree-of-freedom and diversity gain of such channel. The point source will form the element response for various arrays in subsequent sections.

A. Source and Channel Responses

Let us first describe the radiation patterns of polarimetric antenna elements. Fig. 4 shows the radiation patterns of an electric and a magnetic dipole oriented along the z-axis. The magnitude of a radiation pattern reveals the relative strength of the radiated field as a function of the propagation direction. The magnitudes are the same for both dipoles. The difference between them is the direction of the radiated field. For the electric dipole, the direction of the electric field is along $\hat{\boldsymbol{\theta}}$, while for the magnetic dipole, it is along $\hat{\boldsymbol{\phi}}$. That is, the electric field lines due to the electric dipole are the closed paths that circle the torus' hole, while those due to the magnetic dipole are the closed paths that circle the torus' body. In mathematical form, the normalized radiation pattern for the electric dipole is

$$\mathbf{a}_0(\theta,\phi) = \hat{\boldsymbol{\theta}}\sqrt{\tfrac{3}{8\pi}}\sin\theta \tag{1}$$

and that for the magnetic dipole is

$$\mathbf{a}_3(\theta,\phi) = -\hat{\boldsymbol{\phi}}\sqrt{\tfrac{3}{8\pi}}\sin\theta. \tag{2}$$

Note that there are two sets of directions. One denotes the propagation direction (θ,ϕ) where the radiation pattern is a function of it. Another denotes the field direction in terms of unit vectors $\hat{\boldsymbol{\theta}}$ and $\hat{\boldsymbol{\phi}}$ at the propagation direction (θ,ϕ). These unit vectors are functions of (θ,ϕ) as well.

The torus in Fig. 4 revolves about the z-axis. When it revolves about the x-axis, it represents the radiation patterns of an electric and a magnetic dipole oriented along the x-axis, denoted by $\mathbf{a}_1(\theta,\phi)$ and $\mathbf{a}_4(\theta,\phi)$ respectively. Similarly, when the torus revolves about the y-axis, it represents the radiation patterns of an electric and a magnetic dipole oriented along the y-axis, denoted by $\mathbf{a}_2(\theta,\phi)$ and $\mathbf{a}_5(\theta,\phi)$ respectively. As a result, the response of a polarimetric antenna element is given in (3) at the bottom of the page. In the transmit coordinate system, the transmit dipoles

$$\begin{aligned}\mathbf{A}(\theta,\phi) &= [\,\mathbf{a}_0(\theta,\phi) \quad \cdots \quad \mathbf{a}_5(\theta,\phi)\,] \\ &= \sqrt{\frac{3}{8\pi}}\,[\,\hat{\boldsymbol{\theta}} \quad \hat{\boldsymbol{\phi}}\,]\begin{bmatrix} \sin\theta & -\cos\theta\cos\phi & -\cos\theta\sin\phi & 0 & \sin\phi & -\cos\phi \\ 0 & \sin\phi & -\cos\phi & -\sin\theta & \cos\theta\cos\phi & \cos\theta\sin\phi \end{bmatrix}\end{aligned} \tag{3}$$

are co-located at the origin. Similarly, the receive dipoles are co-located at the origin of the receive coordinate system. They both have the same response $\mathbf{A}(\theta,\phi)$. The receive coordinate system is simply a translation transformation of the transmit coordinate system.

The translation operation between the transmit and the receive coordinate system, and scatterers in between the transmit and the receive antennas are captured by the channel response. We consider multipath channels with L physical paths. Scatterers on the lth path affect the radiated field departing at angle $(\theta_{t,l},\phi_{t,l})$. The lth path arrives at the receiver at angle $(\theta_{r,l},\phi_{r,l})$. Path delay and dielectric properties of scatterers introduce a phase change of $\beta_{\hat{\boldsymbol{\theta}}\hat{\boldsymbol{\theta}}}(\theta_{r,l},\phi_{r,l},\theta_{t,l},\phi_{t,l})$ on radiated field oscillating along $\hat{\boldsymbol{\theta}}$ and incident field along $\hat{\boldsymbol{\theta}}$, and the corresponding path gain is $\alpha_{\hat{\boldsymbol{\theta}}\hat{\boldsymbol{\theta}}}(\theta_{r,l},\phi_{r,l},\theta_{t,l},\phi_{t,l})$. Similar definitions apply to the other pairs of field directions. Consequently, the 6×6 multiple-antenna channel matrix $\mathbf{H}$ can be written as

$$\mathbf{H} = \frac{1}{\sqrt{L}}\sum_{l=0}^{L-1}\mathbf{A}^{\dagger}(\theta_{r,l},\phi_{r,l})\,\mathbf{C}(\theta_{r,l},\phi_{r,l},\theta_{t,l},\phi_{t,l})\,\mathbf{A}(\theta_{t,l},\phi_{t,l}) \tag{4}$$

where $\mathbf{C}(\theta_r,\phi_r,\theta_t,\phi_t)$ is a 2×2 matrix with elements:

$$\begin{aligned}
C_{11}(\theta_r,\phi_r,\theta_t,\phi_t) &= \alpha_{\hat{\boldsymbol{\theta}}\hat{\boldsymbol{\theta}}}(\theta_r,\phi_r,\theta_t,\phi_t)e^{j\beta_{\hat{\boldsymbol{\theta}}\hat{\boldsymbol{\theta}}}(\theta_r,\phi_r,\theta_t,\phi_t)}\\
C_{12}(\theta_r,\phi_r,\theta_t,\phi_t) &= \alpha_{\hat{\boldsymbol{\theta}}\hat{\boldsymbol{\phi}}}(\theta_r,\phi_r,\theta_t,\phi_t)e^{j\beta_{\hat{\boldsymbol{\theta}}\hat{\boldsymbol{\phi}}}(\theta_r,\phi_r,\theta_t,\phi_t)}\\
C_{21}(\theta_r,\phi_r,\theta_t,\phi_t) &= \alpha_{\hat{\boldsymbol{\phi}}\hat{\boldsymbol{\theta}}}(\theta_r,\phi_r,\theta_t,\phi_t)e^{j\beta_{\hat{\boldsymbol{\phi}}\hat{\boldsymbol{\theta}}}(\theta_r,\phi_r,\theta_t,\phi_t)}\\
C_{22}(\theta_r,\phi_r,\theta_t,\phi_t) &= \alpha_{\hat{\boldsymbol{\phi}}\hat{\boldsymbol{\phi}}}(\theta_r,\phi_r,\theta_t,\phi_t)e^{j\beta_{\hat{\boldsymbol{\phi}}\hat{\boldsymbol{\phi}}}(\theta_r,\phi_r,\theta_t,\phi_t)}.
\end{aligned}$$

To model the statistical properties of the channel matrix, we adapt Clark's model for fading channels [7]. When there are many scatterers and they are far away from the transceivers, the phases $\beta_{\cdot,\cdot}(\theta_r,\phi_r,\theta_t,\phi_t)$'s are presumably uniformly distributed in $[0,2\pi]$, independently distributed across $(\theta_r,\phi_r,\theta_t,\phi_t)$, and independent of each other. By the Central Limit Theorem, it is reasonable to model the channel matrix $\mathbf{H}$ as a zero mean, jointly Gaussian matrix. The covariance between H_{mn} and $H_{m'n'}$ is

$$\mathrm{Cov}\big(H_{mn},H_{m'n'}\big) = \mathrm{E}_{\theta_{\cdot,\cdot},\phi_{\cdot,\cdot}}\Big[\mathrm{E}_{\beta_{\cdot,\cdot}}\big[H_{mn}H^{*}_{m'n'}\big]\Big] \tag{5}$$

in which the inner expectation is given by

$$\begin{aligned}
&\mathrm{E}_{\beta_{\cdot,\cdot}}\big[H_{mn}H^{*}_{m'n'}\big]\\
=\;&\mathrm{E}\big[|\alpha_{\hat{\boldsymbol{\theta}}\hat{\boldsymbol{\theta}}}(\theta_r,\phi_r,\theta_t,\phi_t)|^2\big]\\
&\quad a^{*}_{m\hat{\boldsymbol{\theta}}}(\theta_r,\phi_r)a_{m'\hat{\boldsymbol{\theta}}}(\theta_r,\phi_r)\,a_{n\hat{\boldsymbol{\theta}}}(\theta_t,\phi_t)a^{*}_{n'\hat{\boldsymbol{\theta}}}(\theta_t,\phi_t)\\
&+\mathrm{E}\big[|\alpha_{\hat{\boldsymbol{\theta}}\hat{\boldsymbol{\phi}}}(\theta_r,\phi_r,\theta_t,\phi_t)|^2\big]\\
&\quad a^{*}_{m\hat{\boldsymbol{\theta}}}(\theta_r,\phi_r)a_{m'\hat{\boldsymbol{\theta}}}(\theta_r,\phi_r)\,a_{n\hat{\boldsymbol{\phi}}}(\theta_t,\phi_t)a^{*}_{n'\hat{\boldsymbol{\phi}}}(\theta_t,\phi_t)\\
&+\mathrm{E}\big[|\alpha_{\hat{\boldsymbol{\phi}}\hat{\boldsymbol{\theta}}}(\theta_r,\phi_r,\theta_t,\phi_t)|^2\big]\\
&\quad a^{*}_{m\hat{\boldsymbol{\phi}}}(\theta_r,\phi_r)a_{m'\hat{\boldsymbol{\phi}}}(\theta_r,\phi_r)\,a_{n\hat{\boldsymbol{\theta}}}(\theta_t,\phi_t)a^{*}_{n'\hat{\boldsymbol{\theta}}}(\theta_t,\phi_t)\\
&+\mathrm{E}\big[|\alpha_{\hat{\boldsymbol{\phi}}\hat{\boldsymbol{\phi}}}(\theta_r,\phi_r,\theta_t,\phi_t)|^2\big]\\
&\quad a^{*}_{m\hat{\boldsymbol{\phi}}}(\theta_r,\phi_r)a_{m'\hat{\boldsymbol{\phi}}}(\theta_r,\phi_r)\,a_{n\hat{\boldsymbol{\phi}}}(\theta_t,\phi_t)a^{*}_{n'\hat{\boldsymbol{\phi}}}(\theta_t,\phi_t)
\end{aligned}$$

where $\mathbf{a}_{m\hat{\boldsymbol{\theta}}}(\theta,\phi)$ and $\mathbf{a}_{m\hat{\boldsymbol{\phi}}}(\theta,\phi)$ are the $\hat{\boldsymbol{\theta}}$ and $\hat{\boldsymbol{\phi}}$ components of $\mathbf{a}_m(\theta,\phi)$. The outer expectation depends on the distribution of physical paths. In a fully-scattered environment, (θ_r,ϕ_r) and (θ_t,ϕ_t) are independent, and are uniformly distributed on a sphere. In an azimuth-scattered environment, they are uniformly distributed on $\big\{(\theta,\phi):0\le\phi<2\pi,\frac{\pi}{2}-\frac{\Delta}{2}\le\theta<\frac{\pi}{2}+\frac{\Delta}{2}\big\}$ for Δ small which is a band centered at the equator.

When physical paths are created due to specular reflection, the incident and the reflected field direction would not change. That is, $\alpha_{\hat{\boldsymbol{\theta}}\hat{\boldsymbol{\phi}}}(\theta_r,\phi_r,\theta_t,\phi_t)=\alpha_{\hat{\boldsymbol{\phi}}\hat{\boldsymbol{\theta}}}(\theta_r,\phi_r,\theta_t,\phi_t)=0$, and $\alpha_{\hat{\boldsymbol{\theta}}\hat{\boldsymbol{\theta}}}(\theta_r,\phi_r,\theta_t,\phi_t)=\alpha_{\hat{\boldsymbol{\phi}}\hat{\boldsymbol{\phi}}}(\theta_r,\phi_r,\theta_t,\phi_t)$. On the other hand, when physical paths are created due to diffused scattering, the incident and the reflected field direction can be totally uncorrelated. That is, all the $\mathrm{E}\big[|\alpha_{\cdot,\cdot}(\theta_r,\phi_r,\theta_t,\phi_t)|^2\big]$'s are equal. In general, physical paths are created by a combination of reflection and scattering. We therefore assume that

$$\begin{aligned}
\mathrm{E}\big[|\alpha_{\hat{\boldsymbol{\theta}}\hat{\boldsymbol{\theta}}}(\theta_r,\phi_r,\theta_t,\phi_t)|^2\big] &= \mathrm{E}\big[|\alpha_{\hat{\boldsymbol{\phi}}\hat{\boldsymbol{\phi}}}(\theta_r,\phi_r,\theta_t,\phi_t)|^2\big] = 1\\
\mathrm{E}\big[|\alpha_{\hat{\boldsymbol{\theta}}\hat{\boldsymbol{\phi}}}(\theta_r,\phi_r,\theta_t,\phi_t)|^2\big] &= \mathrm{E}\big[|\alpha_{\hat{\boldsymbol{\phi}}\hat{\boldsymbol{\theta}}}(\theta_r,\phi_r,\theta_t,\phi_t)|^2\big] = \chi,
\end{aligned}$$

where $0\le\chi\le 1$ is the cross polarization discrimination (XPD). In a channel where diffused scattering is more severe than specular reflection, χ is close to 1. When reflection is more severe than scattering, χ is close to 0.

B. Degree-of-Freedom and Diversity Gain

In both fully-scattered and azimuth-scattered environments, nonzero elements of $\mathbf{H}$ are independent. The variance of the elements of $\mathbf{H}$ is given by:

- *Fully-scattered*

$$\mathrm{Var}(\mathbf{H}) = \begin{bmatrix} 1 & \frac{1}{4} & \frac{1}{4} & 0 & \frac{3}{4} & \frac{3}{4}\\ \frac{1}{4} & \frac{1}{4} & \frac{1}{4} & \frac{3}{4} & \frac{1}{4} & \frac{1}{4}\\ \frac{1}{4} & \frac{1}{4} & \frac{1}{4} & \frac{3}{4} & \frac{1}{4} & \frac{1}{4}\\ 0 & \frac{3}{4} & \frac{3}{4} & 1 & \frac{1}{4} & \frac{1}{4}\\ \frac{3}{4} & \frac{1}{4} & \frac{1}{4} & \frac{1}{4} & \frac{1}{4} & \frac{1}{4}\\ \frac{3}{4} & \frac{1}{4} & \frac{1}{4} & \frac{1}{4} & \frac{1}{4} & \frac{1}{4} \end{bmatrix} + \chi\begin{bmatrix} 0 & \frac{3}{4} & \frac{3}{4} & 1 & \frac{1}{4} & \frac{1}{4}\\ \frac{3}{4} & \frac{3}{4} & \frac{3}{4} & \frac{1}{4} & \frac{1}{4} & \frac{1}{4}\\ \frac{3}{4} & \frac{3}{4} & \frac{3}{4} & \frac{1}{4} & \frac{1}{4} & \frac{1}{4}\\ 1 & \frac{1}{4} & \frac{1}{4} & 0 & \frac{3}{4} & \frac{3}{4}\\ \frac{1}{4} & \frac{1}{4} & \frac{1}{4} & \frac{3}{4} & \frac{3}{4} & \frac{3}{4}\\ \frac{1}{4} & \frac{1}{4} & \frac{1}{4} & \frac{3}{4} & \frac{3}{4} & \frac{3}{4} \end{bmatrix}. \tag{6}$$

- *Azimuth-scattered*

$$\mathrm{Var}(\mathbf{H}) = \frac{9\Delta^2}{64}\begin{bmatrix} 4 & 0 & 0 & 0 & 2 & 2\\ 0 & 1 & 1 & 2 & 0 & 0\\ 0 & 1 & 1 & 2 & 0 & 0\\ 0 & 2 & 2 & 4 & 0 & 0\\ 2 & 0 & 0 & 0 & 1 & 1\\ 2 & 0 & 0 & 0 & 1 & 1 \end{bmatrix} + \chi\frac{9\Delta^2}{64}\begin{bmatrix} 0 & 2 & 2 & 4 & 0 & 0\\ 2 & 0 & 0 & 0 & 1 & 1\\ 2 & 0 & 0 & 0 & 1 & 1\\ 4 & 0 & 0 & 0 & 2 & 2\\ 0 & 1 & 1 & 2 & 0 & 0\\ 0 & 1 & 1 & 2 & 0 & 0 \end{bmatrix} + O(\Delta^3). \tag{7}$$

Both variance matrices are full rank. Therefore, the degree-of-freedom gain in both channels are the same and equal to 6. The co-located orthogonal dipoles are used to resolve both field directions and propagation direction of physical paths.

In the fully-scattered environment, when $\chi = 1$, elements of $\mathbf{H}$ are i.i.d. complex Gaussian random variables. The channel is equivalent to the i.i.d. Rayleigh fading MIMO channel. It attains the full diversity gain. When $\chi = 0$, only two elements of $\mathbf{H}$ become zero. The diversity order decreases from 36 to 34. Cross polarization has only minor effect on the diversity gain. In the azimuth-scattered environment, on the other hand, half of the entries in $\mathbf{H}$ are close to zero when $\chi = 0$. Thus, cross polarization has significant effect on the diversity gain.

III. Linear Arrays

We will first use sampling argument to derive the set of resolvable angular cells for linear arrays. Then, we will look into the degree-of-freedom gain from a pair of transmit and receive resolvable angular cell.

A. Resolvable Angular Cells

For simplicity, we first consider an array of electric dipoles where each dipole is pointing in the z direction. The radiation pattern due to a dipole at the origin is $\mathbf{a}_0(\theta, \phi)$, and that due to a dipole at (x, y, z) close to the origin is

$$e^{i2\pi(x\sin\theta\cos\phi + y\sin\theta\sin\phi + z\cos\theta)}\mathbf{a}_0(\theta,\phi)$$

where all the position parameters x, y, and z, are normalized to a wavelength. Now, if the linear array is oriented along the z-axis, the total electric field due to an array of length L normalized to a wavelength will be

$$\boldsymbol{\mathcal{E}}(\theta,\phi) = \int_{-L/2}^{L/2} s(z)e^{i2\pi z\cos\theta}dz\mathbf{a}_0(\theta,\phi) \tag{8a}$$

$$= S(\cos\theta)\mathbf{a}_0(\theta,\phi) \tag{8b}$$

where $s(z)$ is the signal on the electric dipole at z on the array. Notes that $s(z)$ and $S(\cos\theta)$ are Fourier transform pair. The linear array can only resolve the θ direction. As the range of propagation directions resolvable by the array is $\cos\theta \in [-1, 1]$, the optimal separation between adjacent antenna elements should equal to the inverse of the length of the resolvable interval which is $1/2$ and corresponds to the half wavelength antenna spacing. With this optimal spacing, we can re-write the total electric field as

$$\boldsymbol{\mathcal{E}}(\theta,\phi) = \frac{1}{\sqrt{n}}\sum_{m=0}^{n-1} s_m e^{i\pi m\cos\theta}\mathbf{a}_0(\theta,\phi) \tag{9}$$

where s_m is the signal on the mth dipole. In the expression, the total number of antenna elements is $n = 2L$. When s_m's are all equal to unity, the magnitude of the total electric field in the direction (θ, ϕ) satisfies

$$\left|\boldsymbol{\mathcal{E}}(\theta,\phi)\right|^2 = \frac{1}{n}\left|\frac{\sin(\frac{\pi n}{2}\cos\theta)}{\sin(\frac{\pi}{2}\cos\theta)}\right|^2\left|\mathbf{a}_0(\theta,\phi)\right|^2. \tag{10}$$

It peaks at $\cos\theta = 0$ and is 0 at $\cos\theta = \pm\frac{2k}{n} = \pm\frac{k}{L}$ for $k = 1, \ldots, L$. The angular separation between the peak and the zero crossing is $\frac{1}{L}$ which is the angular resolution of the array.

Suppose the normalized length of the transmit and the receive array are L_t and L_r respectively. Then, the resolvable angular cells at the transmitter and those at the receiver are given by

$$\mathcal{R}_k = \left\{(\theta,\phi) : \frac{k}{L_r} \le \cos\theta < \frac{k+1}{L_r},\ 0 \le \phi < 2\pi\right\} \tag{11a}$$

$$\mathcal{T}_l = \left\{(\theta,\phi) : \frac{l}{L_t} \le \cos\theta < \frac{l+1}{L_t}, 0 \le \phi < 2\pi\right\} \tag{11b}$$

respectively for all k and l, where $n_t = 2L_t$ and $n_r = 2L_r$. Similar to (4), the response between the kth resolvable cell at the receiver and the lth resolvable cell at the transmitter is

$$H^a_{kl} = \frac{1}{\sqrt{L_{kl}}}\sum_{\substack{(\theta_{r,i},\phi_{r,i})\in\mathcal{R}_k\\(\theta_{t,i},\phi_{t,i})\in\mathcal{T}_l}} \mathbf{a}_0^\dagger(\theta_{r,i},\phi_{r,i})\mathbf{C}(\theta_{r,i},\phi_{r,i},\theta_{t,i},\phi_{t,i})\mathbf{a}_0(\theta_{t,i},\phi_{t,i})$$

where L_{kl} denotes the number of physical paths departing from $\mathcal{T}_l$ and arriving at $\mathcal{R}_k$. Replacing $\mathbf{a}_0(\cdot,\cdot)$ by $\mathbf{A}(\cdot,\cdot)$ yields the response for the arrays using polarimetric antenna elements. The 6×6 channel matrix between a pair of resolvable angular cells can be written as

$$\mathbf{H}^a_{kl} = \frac{1}{\sqrt{L_{kl}}}\sum_{\substack{(\theta_{r,i},\phi_{r,i})\in\mathcal{R}_k\\(\theta_{t,i},\phi_{t,i})\in\mathcal{T}_l}} \mathbf{A}^\dagger(\theta_{r,i},\phi_{r,i})\mathbf{C}(\theta_{r,i},\phi_{r,i},\theta_{t,i},\phi_{t,i})\mathbf{A}(\theta_{t,i},\phi_{t,i}). \tag{12}$$

As physical paths departing and arriving at different angles are assumed to be independent, and the resolvable angular cells are nonoverlapping, the $\mathbf{H}^a_{kl}$'s are independent for all k and l. The rank of $\mathbf{H}^a_{kl}$ corresponding to resolvable cells that overlap with physical paths gives the degree-of-freedom gain from using polarimetric antenna elements.

In the fully-scattered environment, we consider linear arrays oriented along the z-axis and the resolvable angular cells are given by (11). When physical paths spread over the azimuth angles only, these arrays are perpendicular to the plane of physical paths. The resolution of the array on the physical paths is poor. In the azimuth-scattered environment, we therefore consider linear arrays oriented along the x-axis which are on the plane of physical paths. The resolvable angular cells become

$$\mathcal{R}_k = \left\{(\theta,\phi) : \frac{k}{L_r} \le \cos\phi < \frac{k+1}{L_r},\ 0 \le \theta < \pi\right\} \tag{13a}$$

$$\mathcal{T}_l = \left\{(\theta,\phi) : \frac{l}{L_t} \le \cos\phi < \frac{l+1}{L_t}, 0 \le \theta < \pi\right\}. \tag{13b}$$

B. Degree-of-Freedom and Diversity Gain

In both fully-scattered and azimuth-scattered environments, elements of $\mathbf{H}^a_{kl}$ are not independent. But we can find matrices that transform $\mathbf{H}^a_{kl}$ into a matrix with independent elements. The results are summarized as follows:

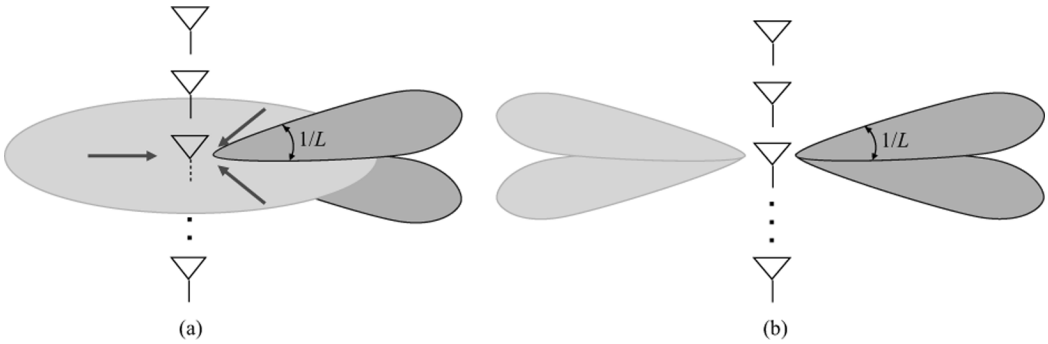

Fig. 5. Illustrates the resolvability of a linear array on physical paths. A linear array can resolve physical paths coming from *different* beams where the beamwidth is the inverse of the length of the array normalized to a wavelength, $1/L$. (a) In a fully-scattered environment, polarimetric antenna elements can resolve physical paths coming from the *same* beam but different directions on the plane perpendicular to the array—the lightly shaded circular region. (b) In an azimuth-scattered environment, polarimetric antenna elements can resolve physical paths coming from the left versus the right of the array within the same beam.

- *Fully-scattered*. There exist 6×6 full-rank matrices $\mathbf{U}_{r,k}$ and $\mathbf{U}_{t,l}$ such that the nonzero elements of $\mathbf{U}_{r,k}^{\dagger}\mathbf{H}_{kl}^{a}\mathbf{U}_{t,l}$ are independent. Its variance matrix is given by

$$\begin{aligned}&\mathrm{Var}\left[\mathbf{U}_{r,k}^{\dagger}\mathbf{H}_{kl}^{a}\mathbf{U}_{t,l}\right]\\&=\frac{9\left(1-\frac{k^2}{L_r^2}\right)\left(1-\frac{l^2}{L_t^2}\right)}{64L_rL_t}\left(\begin{bmatrix}\mathbf{Q}&\mathbf{0}\\\mathbf{0}&\mathbf{Q}\end{bmatrix}+\chi\begin{bmatrix}\mathbf{0}&\mathbf{Q}\\\mathbf{Q}&\mathbf{0}\end{bmatrix}\right)\\&\quad+O\left(\frac{1}{L_r^2L_t}\right)+O\left(\frac{1}{L_rL_t^2}\right)\end{aligned}\tag{14}$$

where

$$\mathbf{Q}=\begin{bmatrix}2\\\frac{1-\frac{k^2}{L_r^2}}{1+\frac{k^2}{L_r^2}}\\\frac{1-\frac{k^2}{L_r^2}}{1+\frac{k^2}{L_r^2}}\end{bmatrix}\begin{bmatrix}2&\frac{1-\frac{l^2}{L_t^2}}{1+\frac{l^2}{L_t^2}}&\frac{1-\frac{l^2}{L_t^2}}{1+\frac{l^2}{L_t^2}}\end{bmatrix}.$$

- *Azimuth-scattered*. There exist 6×6 full-rank matrices $\mathbf{U}_{r,k}$ and $\mathbf{U}_{t,l}$ such that the variance of the elements of $\mathbf{U}_{r,k}^{\dagger}\mathbf{H}_{kl}^{a}\mathbf{U}_{t,l}$ varies as $\mathcal{O}(\Delta)$ and the correlation between the elements varies as $\mathcal{O}(\Delta^3)$. For Δ small, the nonzero elements of $\mathbf{U}_{r,k}^{\dagger}\mathbf{H}_{kl}^{a}\mathbf{U}_{t,l}$ are approximately independent. Its variance matrix is given by

$$\begin{aligned}&\mathrm{Var}\left[\mathbf{U}_{r,k}^{\dagger}\mathbf{H}_{kl}^{a}\mathbf{U}_{t,l}\right]\\&=\frac{9\Delta^2\sqrt{\left(1-\frac{k^2}{L_r^2}\right)\left(1-\frac{l^2}{L_t^2}\right)}}{16\pi^2L_rL_t}\\&\quad\cdot\left(\begin{bmatrix}\mathbf{P}&\mathbf{0}&\mathbf{0}\\\mathbf{0}&\mathbf{P}&\mathbf{0}\\\mathbf{0}&\mathbf{0}&\mathbf{0}\end{bmatrix}+\chi\begin{bmatrix}\mathbf{0}&\mathbf{P}&\mathbf{0}\\\mathbf{P}&\mathbf{0}&\mathbf{0}\\\mathbf{0}&\mathbf{0}&\mathbf{0}\end{bmatrix}\right)\\&\quad+O\left(\frac{\Delta^3}{L_r^2L_t}\right)+O\left(\frac{\Delta^3}{L_rL_t^2}\right)\end{aligned}\tag{15}$$

where

$$\mathbf{P}=\begin{bmatrix}1\\\frac{4\frac{k^2}{L_r^2}}{1-\frac{k^4}{L_r^4}}\end{bmatrix}\begin{bmatrix}1&\frac{4\frac{l^2}{L_t^2}}{1-\frac{l^4}{L_t^4}}\end{bmatrix}.$$

The proof is included in Appendix A.

In the fully-scattered environment, the two submatrices $\mathbf{Q}$ correspond to resolving the field directions, $\hat{\boldsymbol{\theta}}$ and $\hat{\boldsymbol{\phi}}$, which contribute a multiplicative gain of 2. The 3×3 submatrix $\mathbf{Q}$ itself corresponds to resolving physical paths coming from different ϕ directions as shown in Fig. 5(a). This contributes another multiplicative gain of 3. The degree-of-freedom gain is therefore equal to 6.

Similarly, in the azimuth-scattered environment, the two submatrices $\mathbf{P}$ corresponding to resolving the field direction. The 2×2 submatrix $\mathbf{P}$ itself corresponds to resolving physical paths coming from $0\le\phi<\pi$ versus $\pi\le\phi<2\pi$, that is, from the right side versus the left side of the array as shown in Fig. 5(b). The degree-of-freedom gain is 4.

In both channels, when $\chi=0$, the diversity order is reduced by half. Cross polarization improves the diversity gain substantially.

Finally, the number of resolvable cells that overlap with the physical paths is $2L_t$ at the transmitter and $2L_r$ at the receiver in both channels. They are equal to the respective number of antenna elements. Therefore, the number of array degrees of freedom is the minimum of them.

IV. Planar Arrays

Now we extend the sampling argument to higher dimensional Euclidean spaces to derive the resolvable angular cells of planar arrays.

A. Resolvable Angular Cells

Suppose the planar arrays are lying on the xy-plane. Then, the total electric field due to an array of electric dipoles pointing in the z direction can be expressed as

$$\begin{aligned}\boldsymbol{\mathcal{E}}(\theta,\phi)&=\int\int s(x,y)e^{i2\pi(x\sin\theta\cos\phi+y\sin\theta\sin\phi)}\,dxdy\\&\quad\cdot\mathbf{a}_0(\theta,\phi)&\text{(16a)}\\&=S(\sin\theta\cos\phi,\sin\theta\sin\phi)\,\mathbf{a}_0(\theta,\phi).&\text{(16b)}\end{aligned}$$

Defining $\kappa_x=\sin\theta\cos\phi$ and $\kappa_y=\sin\theta\sin\phi$, $s(x,y)$ and $S(\kappa_x,\kappa_y)$ are 2-D Fourier transform pair. As $\kappa_x^2+\kappa_y^2=\sin^2\theta\le 1$, the range of propagation directions resolvable by the array is limited to a unit disk in the (κ_x,κ_y) coordinates. The optimal placement of antenna elements $\mathbf{p_m}$ can be obtained

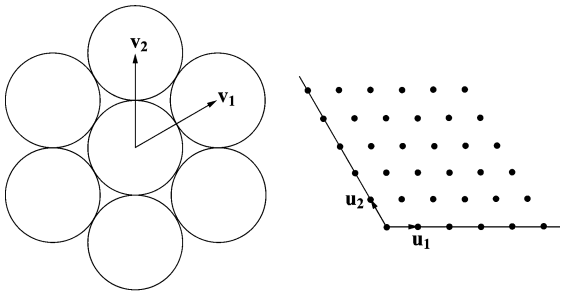

Fig. 6. (a) Illustrates the densest packing of unit disks. (b) Illustrates the optimal placement of antenna elements on a planar array.

from the periodic lattice defined by the densest packing of the unit disk on a plane [8]. Fig. 6(a) illustrates that the densest packing is a hexagonal lattice defined by the vectors $\mathbf{v}_1$ and $\mathbf{v}_2$:

$$\mathbf{v}_1 = \begin{bmatrix} \sqrt{3} \\ 1 \end{bmatrix} \qquad \mathbf{v}_2 = \begin{bmatrix} 0 \\ 2 \end{bmatrix}.$$

The optimal placement of antenna elements is then given by

$$\mathbf{p_m} = m_1\mathbf{u}_1 + m_2\mathbf{u}_2$$

with

$$\mathbf{u}_i^T\mathbf{v}_j = \delta_{ij} \qquad \forall\, i,j = 1,2.$$

The vectors $\mathbf{u}_1$ and $\mathbf{u}_2$ are

$$\mathbf{u}_1 = \begin{bmatrix} \frac{1}{\sqrt{3}} \\ 0 \end{bmatrix} \qquad \mathbf{u}_2 = \begin{bmatrix} -\frac{1}{2\sqrt{3}} \\ \frac{1}{2} \end{bmatrix}.$$

The lattice for the optimal antenna placement is a 120° rhombus shown in Fig. 6(b). Suppose the area of the antenna array is A normalized to the square of a wavelength and there are equal number of antennas on each direction. Then, the total number of antenna elements is $n = 2\sqrt{3}A$

With the optimal placement of antenna elements, we can re-write the total electric field as

$$\boldsymbol{\mathcal{E}}(\theta,\phi) = \frac{1}{\sqrt{n}} \sum_{m_1=0}^{\sqrt{n}-1} \sum_{m_2=0}^{\sqrt{n}-1} s_{\mathbf{m}} e^{i2\pi(m_1\mathbf{u}_1+m_2\mathbf{u}_2)^T(\alpha_1\mathbf{v}_1+\alpha_2\mathbf{v}_2)} \cdot \mathbf{a}_0(\theta,\phi) \tag{17}$$

where $(\kappa_x,\kappa_y) = \alpha_1\mathbf{v}_1 + \alpha_2\mathbf{v}_2$. When $s_{\mathbf{m}}$'s are all equal to unity, the magnitude of the total electric field satisfies

$$\left|\boldsymbol{\mathcal{E}}(\theta,\phi)\right|^2 = \frac{1}{n}\left|\frac{\sin(\pi\alpha_1\sqrt{n})}{\sin(\pi\alpha_1)}\right|^2 \left|\frac{\sin(\pi\alpha_2\sqrt{n})}{\sin(\pi\alpha_2)}\right|^2 \left|\mathbf{a}_0(\theta,\phi)\right|^2. \tag{18}$$

It peaks at $(\alpha_1,\alpha_2) = (0,0)$ and is 0 at

$$(\alpha_1,\alpha_2) = \left(\pm\frac{k_1}{\sqrt{n}}, \pm\frac{k_2}{\sqrt{n}}\right) \qquad k_1,k_2 = 1,\ldots,\frac{\sqrt{n}}{2}.$$

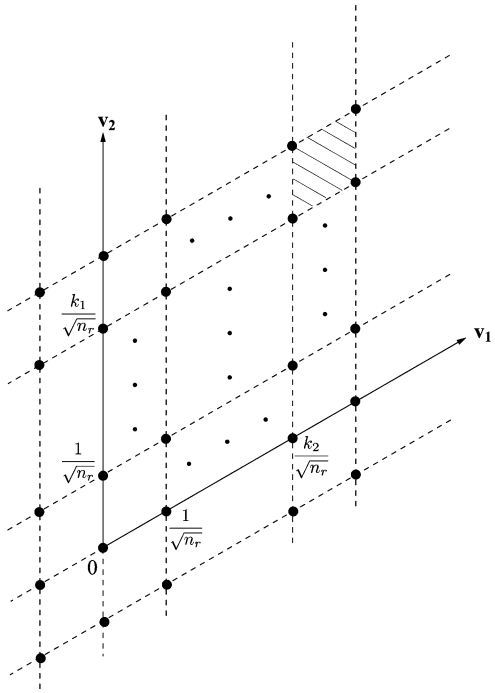

Fig. 7. Illustrates the resolvable angular cells from a rhombus-shaped planar array of length $\sqrt{\frac{n_r}{3}}$. The shaded region is the (k_1,k_2)th resolvable cell.

Suppose the normalized area of the transmit and the receive array are A_t and A_r respectively. Then, the resolvable angular cells at the transmitter and those at the receiver are given by

$$\mathcal{R}_{\mathbf{k}} = \left\{ (\theta,\phi) : \frac{k_1}{\sqrt{\frac{2}{\sqrt{3}}A_r}} \le \sin\theta\cos\phi < \frac{k_1+1}{\sqrt{\frac{2}{\sqrt{3}}A_r}} \right.$$
$$\left. \frac{k_2}{\sqrt{\frac{2}{\sqrt{3}}A_r}} \le \sin\theta\sin(\phi-30^\circ) < \frac{k_2+1}{\sqrt{\frac{2}{\sqrt{3}}A_r}} \right\}$$
$$\mathcal{T}_{\mathbf{l}} = \left\{ (\theta,\phi) : \frac{l_1}{\sqrt{\frac{2}{\sqrt{3}}A_t}} \le \sin\theta\cos\phi < \frac{l_1+1}{\sqrt{\frac{2}{\sqrt{3}}A_t}} \right.$$
$$\left. \frac{l_2}{\sqrt{\frac{2}{\sqrt{3}}A_t}} \le \sin\theta\sin(\phi-30^\circ) < \frac{l_2+1}{\sqrt{\frac{2}{\sqrt{3}}A_t}} \right\}$$

respectively for all $\mathbf{k}$ and $\mathbf{l}$, and are shown in Fig. 7. The 6×6 channel matrix between a pair of resolvable angular cells is similarly given by (12).

B. Degree-of-Freedom and Diversity Gain

Fully-Scattered Channel: Referring to Fig. 7, we denote the (θ,ϕ) coordinates of the left lowest vertex of the (k_1,k_2)th resolvable angular cell by $(\theta_{r,\mathbf{k}},\phi_{r,\mathbf{k}})$ at the receiver. It satisfies

$$\sin\theta_{r,\mathbf{k}} = \sqrt{\frac{k_1^2+k_1k_2+k_2^2}{\frac{\sqrt{3}}{2}A_r}} \tag{19a}$$

$$\tan\phi_{r,\mathbf{k}} = \frac{2}{\sqrt{3}}\left(\frac{k_2}{k_1}+\frac{1}{2}\right). \tag{19b}$$

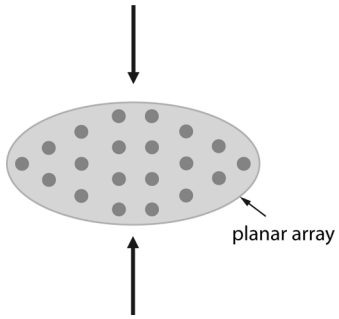

Fig. 8. Planar array with polarimetric antenna elements can resolve physical paths coming from above versus below the array.

Similarly definition applies to $(\theta_{t,\mathbf{l}}, \phi_{t,\mathbf{l}})$ at the transmitter. There exist 6×6 full-rank matrices $\mathbf{U}_{r,\mathbf{k}}$ and $\mathbf{U}_{t,\mathbf{l}}$ such that the variance of the elements of $\mathbf{U}_{r,\mathbf{k}}^{\dagger}\mathbf{H}_{\mathbf{kl}}^{a}\mathbf{U}_{t,\mathbf{l}}$ varies as $\mathcal{O}\left(\frac{1}{A_t A_r}\right)$ and the correlation between the elements varies as $\mathcal{O}\left(\frac{1}{A_t^2 A_r}\right)$ and $\mathcal{O}\left(\frac{1}{A_t A_r^2}\right)$. For A_t and A_r large, the nonzero elements of $\mathbf{U}_{r,\mathbf{k}}^{\dagger}\mathbf{H}_{\mathbf{kl}}^{a}\mathbf{U}_{t,\mathbf{l}}$ are approximately independent. Its variance matrix is given by

$$\begin{aligned}
&\operatorname{Var}\left[\mathbf{U}_{r,\mathbf{k}}^{\dagger}\mathbf{H}_{\mathbf{kl}}^{a}\mathbf{U}_{t,\mathbf{l}}\right] \\
&= \frac{9}{\pi^2 A_r A_t}\frac{\sin^2\theta_{r,\mathbf{k}}}{\sqrt{1-\sin^2\theta_{r,\mathbf{k}}}}\frac{\sin^2\theta_{t,\mathbf{l}}}{\sqrt{1-\sin^2\theta_{t,\mathbf{l}}}} \\
&\quad \cdot \left(\begin{bmatrix}\mathbf{Q} & \mathbf{0} & \mathbf{0}\\ \mathbf{0} & \mathbf{Q} & \mathbf{0}\\ \mathbf{0} & \mathbf{0} & \mathbf{0}\end{bmatrix} + \chi\begin{bmatrix}\mathbf{0} & \mathbf{Q} & \mathbf{0}\\ \mathbf{Q} & \mathbf{0} & \mathbf{0}\\ \mathbf{0} & \mathbf{0} & \mathbf{0}\end{bmatrix}\right) \\
&\quad + O\left(\frac{1}{A_t^2 A_r}\right) + O\left(\frac{1}{A_t A_r^2}\right) \qquad (20)
\end{aligned}$$

where

$$\begin{aligned}
\mathbf{Q} &= \begin{bmatrix} 1 \\ (1-\sin^2\theta_{r,\mathbf{k}})\sin^2\phi_{r,\mathbf{k}}\cos^2\phi_{r,\mathbf{k}}\end{bmatrix} \\
&\quad \cdot \begin{bmatrix} 1 & (1-\sin^2\theta_{t,\mathbf{l}})\sin^2\phi_{t,\mathbf{l}}\cos^2\phi_{t,\mathbf{l}}\end{bmatrix}. \qquad (21)
\end{aligned}$$

The proof is included in Appendix B.

The two submatrices $\mathbf{Q}$ correspond to resolving the field direction, $\hat{\boldsymbol{\theta}}$ and $\hat{\boldsymbol{\phi}}$. The 2×2 submatrix $\mathbf{Q}$ itself corresponds to resolving physical paths coming from $0 \le \theta < \pi/2$ versus $\pi/2 \le \theta < \pi$, that is, from the upper versus the lower side of the array as shown in Fig. 8. The degree-of-freedom gain is therefore 4.

When $\chi = 0$, the diversity order is reduced by half. Cross polarization improves the diversity gain substantially.

Finally, the area of resolvable angular cell is $4 \cdot \frac{\sqrt{3}}{2n_t} = \frac{1}{A_t}$ at the transmitter. The number of resolvable angular cells filling up a unit disk therefore equals to πA_t while the number of antenna elements is $2\sqrt{3}A_t$. The number of antenna elements is slightly larger than the number of resolvable angular cells. For linear arrays, they are the same. The number of array degrees of freedom is determined by the number of resolvable angular cells that overlap with physical paths but not by the number of antenna elements. Therefore, the number of array degrees of freedom for planar arrays is $\min\{\pi A_t, \pi A_r\}$.

Azimuth-Scattered Channel: When the directions of physical paths are limited to $\frac{\pi}{2} - \frac{\Delta}{2} \le \theta < \frac{\pi}{2} + \frac{\Delta}{2}$, it is equivalent to $1 - \frac{\Delta^2}{4} \le |\sin\theta| \le 1$ for Δ small. As $\kappa_x^2 + \kappa_y^2 = \sin^2\theta$, physical paths are clustered on the unit circular ring—the shaded region in Fig. 9(a). Here, we are interested in studying the rank of $\mathbf{H}_{\mathbf{kl}}^{a}$ for those angular resolvable cells that overlap with the circular shaded region. The overlapping region in each resolvable cell is irregular. To ease the derivation, we approximate the circular ring with the largest hexagonal ring that is inside the unit circle—the shaded region in Fig. 9(b).

For $\mathbf{k}$ and $\mathbf{l}$ in the hexagonal ring, there exist 6×6 full-rank matrices $\mathbf{U}_{r,\mathbf{k}}$ and $\mathbf{U}_{t,\mathbf{l}}$ such that the nonzero elements of $\mathbf{U}_{r,\mathbf{k}}^{\dagger}\mathbf{H}_{\mathbf{kl}}^{a}\mathbf{U}_{t,\mathbf{l}}$ are approximately independent for $\frac{\Delta}{\sqrt{A_t}}$, $\frac{\Delta}{\sqrt{A_r}}$ small. Its variance matrix is given by

$$\begin{aligned}
&\operatorname{Var}\left[\mathbf{U}_{r,\mathbf{k}}^{\dagger}\mathbf{H}_{\mathbf{kl}}^{a}\mathbf{U}_{t,\mathbf{l}}\right] \\
&= \frac{6\Delta^2}{\pi^2}\sqrt{\frac{3}{A_r A_t}}\begin{bmatrix}1&0&0&0&0&0\\0&1&0&0&0&0\\0&0&0&0&0&0\\0&0&0&0&0&0\\0&0&0&0&0&0\\0&0&0&0&0&0\end{bmatrix} \\
&\quad + \chi\frac{6\Delta^2}{\pi^2}\sqrt{\frac{3}{A_r A_t}}\begin{bmatrix}0&1&0&0&0&0\\1&0&0&0&0&0\\0&0&0&0&0&0\\0&0&0&0&0&0\\0&0&0&0&0&0\\0&0&0&0&0&0\end{bmatrix} \\
&\quad + O\left(\frac{\Delta^2}{A_t\sqrt{A_r}}\right) + O\left(\frac{\Delta^2}{\sqrt{A_t}A_r}\right) + O\left(\frac{\Delta^3}{\sqrt{A_t A_r}}\right). \qquad (22)
\end{aligned}$$

The proof is included in Appendix B.

The degree-of-freedom gain is 2 and is from resolving the field directions only. When $\chi = 0$, the diversity order is reduced by half. Cross polarization could double the diversity gain. Finally, the number of resolvable angular cells that overlap with the hexagonal ring is $3\sqrt{n_t} = 3\sqrt{2\sqrt{3}A_t}$ at the transmitter. Therefore, the number of array degrees of freedom is approximately equal to $\min\{3\sqrt{2\sqrt{3}A_t}, 3\sqrt{2\sqrt{3}A_r}\} \approx \min\{6\sqrt{A_t}, 6\sqrt{A_r}\}$.

As the number of array degrees of freedom depends on the square root of array area, it suffices to place the antenna elements on the perimeter of the array. This leads us to compare the results with those of linear arrays. Suppose $L_t = \sqrt{A_t}$ and $L_r = \sqrt{A_r}$. The number of array degrees of freedom from using linear arrays is $\min\{2\sqrt{A_t}, 2\sqrt{A_r}\}$, versus $\min\{6\sqrt{A_t}, 6\sqrt{A_r}\}$ from using planar arrays. It is because linear array resolves $\cos\phi$ while planar array resolves ϕ. When polarimetric antenna elements are used, the total number of degrees of freedom is $\min\{8\sqrt{A_t}, 8\sqrt{A_r}\}$ versus $\min\{12\sqrt{A_t}, 12\sqrt{A_r}\}$. The ratio diminishes because linear array with polarimetric antenna elements not only resolves $\cos\phi$ but also it is able to distinguish between $0 \le \phi < \pi$ and $\pi \le \phi < 2\pi$.

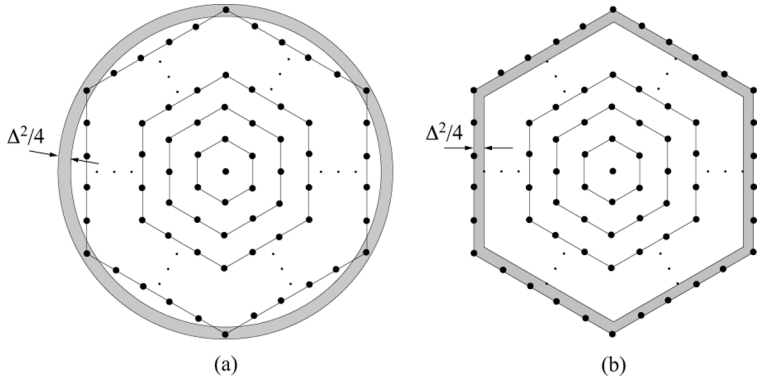

Fig. 9. Illustrates the same resolvable angular cells as in Fig. 7. The lattice points in the angular domain can be connected as concentric hexagons. The outer circle in (a) is a unit circle while the inner circle is of radius $1-\frac{\Delta^2}{4}$. The resolvable angular cells that overlap with this circular ring, convey information, and the corresponding $\mathbf{H}^a_{\mathbf{kl}}$'s are nonzero. The hexagonal ring in (b) is an approximation to the circular ring in (a).

V. Volumetric Arrays

A. Resolvable Angular Cells

Same as in the linear and planar arrays, we first consider an array of electric dipoles pointing in the z direction. The total electric field can be expressed as

$$\begin{aligned}&\boldsymbol{\mathcal{E}}(\theta,\phi)\\&=\int\int\int s(x,y,z)e^{i2\pi(x\sin\theta\cos\phi+y\sin\theta\sin\phi+z\cos\theta)}dxdydz\\&\quad\cdot\mathbf{a}_0(\theta,\phi)\qquad(23a)\\&=S(\sin\theta\cos\phi,\sin\theta\sin\phi,\cos\theta)\mathbf{a}_0(\theta,\phi).\qquad(23b)\end{aligned}$$

Defining $\kappa_x=\sin\theta\cos\phi$, $\kappa_y=\sin\theta\sin\phi$, and $\kappa_z=\cos\theta$, $s(x,y,z)$ and $S(\kappa_x,\kappa_y,\kappa_z)$ are 3-D Fourier transform pair. Now, $\kappa_x^2+\kappa_y^2+\kappa_z^2=1$. The range of propagation directions resolvable by the array is limited to a spherical shell of unit radius in the $(\kappa_x,\kappa_y,\kappa_z)$ coordinates.

In the planar array, when physical paths spread over the azimuth angles only, (κ_x,κ_y) is limited to a unit *circle*. We used the resolvable angular cells for the case when (κ_x,κ_y) is limited to a unit circular *disk*, and then focused on the resolvable angular cells that overlap with the unit circle, as illustrated in Fig. 9(a). For the volumetric array, $(\kappa_x,\kappa_y,\kappa_z)$ is limited to a spherical *shell* of unit radius. We use the same approach as in the planar array. We will first obtain the resolvable angular cells for the case when $(\kappa_x,\kappa_y,\kappa_z)$ is limited to a unit *sphere*, and then focus on the resolvable angular cells that overlap with the unit spherical shell.

The optimal placement of antenna elements $\mathbf{p_m}$ is determined by the densest packing of the unit sphere. Both hexagonal close packing and cubic close packing yield the maximum possible packing density. We consider the cubic close packing lattice because it can be constructed by integer combination of the following three vectors:

$$\mathbf{v}_1=\begin{bmatrix}\sqrt{2}\\\sqrt{2}\\0\end{bmatrix}\qquad\mathbf{v}_2=\begin{bmatrix}-\sqrt{2}\\0\\\sqrt{2}\end{bmatrix}\qquad\mathbf{v}_3=\begin{bmatrix}\sqrt{2}\\-\sqrt{2}\\0\end{bmatrix}.$$

Thus, the antenna locations are given by

$$\mathbf{p_m}=m_1\mathbf{u}_1+m_2\mathbf{u}_2+m_3\mathbf{u}_3$$

where

$$\mathbf{u}_1=\begin{bmatrix}\frac{1}{2\sqrt{2}}\\\frac{1}{2\sqrt{2}}\\\frac{1}{2\sqrt{2}}\end{bmatrix}\qquad\mathbf{u}_2=\begin{bmatrix}0\\0\\\frac{1}{\sqrt{2}}\end{bmatrix}\qquad\mathbf{u}_3=\begin{bmatrix}\frac{1}{2\sqrt{2}}\\-\frac{1}{2\sqrt{2}}\\\frac{1}{2\sqrt{2}}\end{bmatrix}.$$

Suppose the volume of the antenna array is V normalized to the cube of a wavelength and there are equal number of antennas on each direction. Then, the total number of antenna elements is $n=4\sqrt{2}V$.

With the optimal placement of antenna elements, the resolvable angular cells at the transmitter and those at the receiver are defined by the following lattices:

$$\left\{\mathbf{e}_r\left(\frac{k_1}{\sqrt[3]{n_r}}\mathbf{v}_1+\frac{k_2}{\sqrt[3]{n_r}}\mathbf{v}_2+\frac{k_3}{\sqrt[3]{n_r}}\mathbf{v}_3\right):k_1,k_2,k_3=-\frac{\sqrt[3]{n_r}}{2}\right.\\\left.\ldots,\frac{\sqrt[3]{n_r}}{2}-1\right\}\qquad(24a)$$

$$\left\{\mathbf{e}_t\left(\frac{l_1}{\sqrt[3]{n_r}}\mathbf{v}_1+\frac{l_2}{\sqrt[3]{n_r}}\mathbf{v}_2+\frac{l_3}{\sqrt[3]{n_r}}\mathbf{v}_3\right):l_1,l_2,l_3=-\frac{\sqrt[3]{n_r}}{2}\right.\\\left.\ldots,\frac{\sqrt[3]{n_r}}{2}-1\right\}\qquad(24b)$$

respectively, where V_t and V_r are the normalized volume of the transmit and the receive array respectively. Fig. 10 shows one of the resolvable angular cells at the receiver.

B. Degree-of-Freedom and Diversity Gain

When physical paths spread over all directions, we study the rank of $\mathbf{H}^a_{\mathbf{kl}}$ for those resolvable angular cells that overlap with the unit spherical shell. When physical paths spread over the azimuth angles only, we study those cells that overlap with the unit circle on the xy-plane. The analyses are similar to those of planar arrays in the azimuth-scattered environment. The rank of $\mathbf{H}^a_{\mathbf{kl}}$ at the overlapped cells is 2 which corresponds to resolving the field directions, $\hat{\boldsymbol{\theta}}$ and $\hat{\boldsymbol{\phi}}$. Furthermore, cross polarization could double the diversity gain.

In the fully-scattered environment, we count the number of resolvable cells that overlap with the unit spherical shell to compute the number of array degrees of freedom. Each resolvable

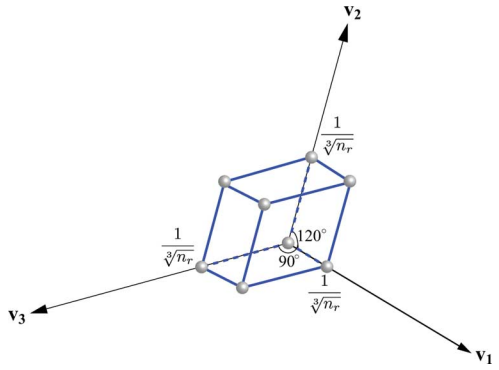

Fig. 10. Illustrates a resolvable angular cell from a parallelepiped volumetric array.

cell has 6 faces. At the transmitter, two of them are of area $4n_t^{-2/3}$ and the remaining four have area of $2\sqrt{3}n_t^{-2/3}$. Therefore, the number of overlapped cells is bounded between $\pi n_t^{2/3}$ and $\frac{2\pi}{\sqrt{3}}n_t^{2/3}$, and is approximately equal to $\pi n_t^{2/3}$. Hence, the number of array degrees of freedom is approximately equal to $\min\left\{2\pi\sqrt[3]{32}V_t^{2/3}, 2\pi\sqrt[3]{32}V_r^{2/3}\right\}\approx \min\left\{20V_t^{2/3}, 20V_r^{2/3}\right\}$.

In the azimuth-scattered environment, we count the number of resolvable cells that overlap with the unit circle instead. The sides of each resolvable cell have the same length equal to $\frac{2}{\sqrt[3]{n_t}}$ at the transmitter. The number of overlapped cells is $\pi\sqrt[3]{n_t}$. Therefore, the number of array degrees of freedom is approximately equal to $\min\left\{2\pi\sqrt[3]{4\sqrt{2}}V_t^{1/3}, 2\pi\sqrt[3]{4\sqrt{2}}V_r^{1/3}\right\}\approx \min\{11V_t^{1/3}, 11V_r^{1/3}\}$.

VI. A Physical Approach

Up to this point, our reasoning is based on resolvable angular cells. These cells are derived from the sampling approach. It works well when the portion of a resolvable cell that overlaps with the physical paths is the same across all overlapped cells. When they are not the same such as planar arrays in azimuth-scattered environment and volumetric arrays, the sampling approach gives accurate result for the degree-of-freedom gain from using polarimetric antenna elements but gives approximated result for the number of array degrees of freedom. To obtain accurate result for the array degrees of freedom, we should use a physical approach based on vector multipole decomposition. This approach also illustrates the transition of the degree-of-freedom gain from 6 for point sources to 2 for volumetric arrays from using polarimetric antenna elements.

A. Source and Channel Responses

With reference to (23a), the radiated electric field due to an arbitrary source region can be expressed as

$$\boldsymbol{\mathcal{E}}(\theta,\phi) = \int\int\int \mathbf{A}(\theta,\phi)\,\mathbf{s}(x,y,z) \cdot e^{i2\pi(x\sin\theta\cos\phi + y\sin\theta\sin\phi + z\cos\theta)}\,dxdydz \quad (25)$$

where $\mathbf{s}(x,y,z)$ is a 6×1 functional and its ith element denotes the signal on the ith co-located orthogonal dipole at (x,y,z) on the array. The expression only captures the radiated field. A complete expression that is valid in all field regions, is in terms of the free-space dyadic Green function as follows:

$$\boldsymbol{\mathcal{E}}(\theta,\phi) = i\omega\mu_0 \int \mathbf{G}(\mathbf{r},\mathbf{r}')\mathbf{s}(\mathbf{r}')\,d\mathbf{r}' \quad (26)$$

where $\mathbf{s}(\mathbf{r})$ becomes a 3×1 functional and denotes the current at $\mathbf{r}$ in the source region. The dyadic Green function can be written as

$$\mathbf{G}(\mathbf{r},\mathbf{r}') = \left(\mathbf{I} + \frac{\nabla\nabla}{k_0^2}\right) g(\mathbf{r},\mathbf{r}') \text{ and } g(\mathbf{r},\mathbf{r}') = \frac{e^{ik_0|\mathbf{r}-\mathbf{r}'|}}{4\pi|\mathbf{r}-\mathbf{r}'|} \quad (27)$$

where k_0 is the wavenumber. It is a linear operator and can be decomposed into its spectral elements as

$$\mathbf{G}(\mathbf{r},\mathbf{r}') = \sum_m \sigma_m \mathbf{u}_m(\mathbf{r})\mathbf{v}_m(\mathbf{r}') \quad (28)$$

where $\mathbf{u}_m(\mathbf{r})$ and $\mathbf{v}_m(\mathbf{r})$ are the mth eigenvectors, and σ_m is the corresponding singular value. Now if we project the input signal $\mathbf{s}(\mathbf{r})$ onto the set of orthonormal basis $\{\mathbf{v}(\mathbf{r})\}$, the electric field can be written in terms of $\mathbf{u}_m(\mathbf{r})$

$$\boldsymbol{\mathcal{E}}(\theta,\phi) = \sum_{m=0}^{n-1} s_m\sigma_m\mathbf{u}_m(\mathbf{r}) \quad (29)$$

where s_m is the projection of $\mathbf{s}(\mathbf{r})$ onto $\mathbf{v}_m(\mathbf{r})$. The expression is similar to (9) and (17) where the discrete representations are based on sampling. Here, it is based on multipole decomposition.

To model the channel, we project all scatterers affecting the radiated field onto a sphere of radius R_s enclosing the transmit array. Similarly, we project all scatterers affecting the incident field onto a sphere of radius R_s enclosing the receive array. The choice of R_s makes sure that scatterers are in the far field of both transmit and receive array. Consequently, the response between the mth receive eigenvector and the nth transmit eigenvector is

$$H_{mn} = \frac{1}{\sqrt{L}}\sum_{l=0}^{L}\sigma_{r,m}\sigma_{t,n}\mathbf{u}_{r,m}^{\dagger}(R_s\hat{\boldsymbol{\kappa}}_{r,l})\mathbf{C}(\hat{\boldsymbol{\kappa}}_{r,l},\hat{\boldsymbol{\kappa}}_{t,l}) \mathbf{u}_{t,n}(R_s\hat{\boldsymbol{\kappa}}_{t,l}) \quad (30)$$

for $m=0,\ldots,n_r-1$ and $n=0,\ldots,n_t-1$, where $\hat{\boldsymbol{\kappa}}_{r,l}$ and $\hat{\boldsymbol{\kappa}}_{t,l}$ are the direction of arrival and direction of departure of the lth physical path respectively. Assume $\chi=1$. The covariance between H_{mn} and $H_{n'm'}$ is

$$\begin{aligned}\mathrm{E}\left[H_{mn}H_{m'n'}^{*}\right] &= \sigma_{r,m}\sigma_{t,n}\sigma_{r,m'}\sigma_{t,n'} \\ &\quad\cdot \mathrm{E}_{\hat{\boldsymbol{\kappa}}_r}\left[\mathbf{u}_{r,m}^{\dagger}(R_s\hat{\boldsymbol{\kappa}}_r)\mathbf{u}_{r,m'}(R_s\hat{\boldsymbol{\kappa}}_r)\right] \\ &\quad\cdot \mathrm{E}_{\hat{\boldsymbol{\kappa}}_t}\left[\mathbf{u}_{t,n'}^{\dagger}(R_s\hat{\boldsymbol{\kappa}}_t)\mathbf{u}_{t,n}(R_s\hat{\boldsymbol{\kappa}}_t)\right]. \end{aligned} \quad (31)$$

Suppose $\boldsymbol{\Sigma}_r$ is a $n_r\times n_r$ diagonal matrix with mth diagonal element equal to $\sigma_{r,m}$, $\mathbf{U}_r(\mathbf{r})$ is a $3\times n_r$ functional matrix with mth column being $\mathbf{u}_{r,m}(\mathbf{r})$, and $\mathbf{V}_r(\mathbf{r})$ is a $3\times n_r$ functional matrix with mth column being $\mathbf{v}_{r,m}(\mathbf{r})$. Similar definitions apply to

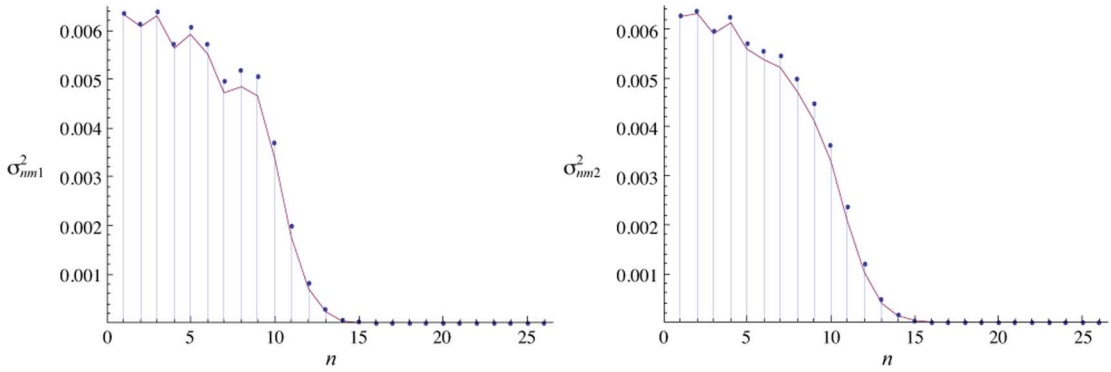

Fig. 11. Plots the distribution of σ^2_{nml} for R equal to 2 wavelength and $R_s = 2R$. The connected line corresponds to approximating $|h_n^{(1)}(k_0 R_s)|$ by $\frac{1}{k_0 R_s}$.

$\mathbf{\Sigma}_t$, $\mathbf{U}_t(\mathbf{r})$, and $\mathbf{V}_t(\mathbf{r})$. Then, the number of degrees of freedom is given by

$$\begin{aligned}\text{d.o.f.} = \min \text{rank}\Big\{&\mathbf{\Sigma}_r, \mathbf{\Sigma}_t, \mathrm{E}_{\hat{\boldsymbol{\kappa}}_r}\left[\mathbf{U}_r^\dagger(R_s\hat{\boldsymbol{\kappa}}_r)\mathbf{U}_r(R_s\hat{\boldsymbol{\kappa}}_r)\right]\\ &\mathrm{E}_{\hat{\boldsymbol{\kappa}}_t}\left[\mathbf{U}_t^\dagger(R_s\hat{\boldsymbol{\kappa}}_t)\mathbf{U}_t(R_s\hat{\boldsymbol{\kappa}}_t)\right], \int_{\mathcal{V}_r}\mathbf{V}_r^\dagger(\mathbf{r})\mathbf{V}_r(\mathbf{r})d\mathbf{r}\\ &\int_{\mathcal{V}_r}\mathbf{V}_r^\dagger(\mathbf{r})\mathbf{V}_r(\mathbf{r})\,d\mathbf{r}, \int_{\mathcal{V}_t}\mathbf{V}_t^\dagger(\mathbf{r})\mathbf{V}_t(\mathbf{r})d\mathbf{r}\Big\}. \end{aligned} \quad (32)$$

The $\mathcal{V}_r$ and $\mathcal{V}_t$ define the transmit and the receive source region respectively. When the source region is a sphere, the two integrals equal to an identity matrix due to the orthonormal property of $\mathbf{v}_m(\mathbf{r})$'s. In a fully-scattered environment, the two expectations equal to an identity matrix due to the orthonormal property of $\mathbf{u}_m(\mathbf{r})$'s. The number of degrees of freedom simplifies to $\min\ \text{rank}\{\mathbf{\Sigma}_r, \mathbf{\Sigma}_t\}$. Next, we derive the distribution of the singular values, and hence obtain the rank of $\mathbf{\Sigma}_r$ and $\mathbf{\Sigma}_t$.

B. Vector Multipole Decomposition

The dyadic Green function can be decomposed into a sum of vector multipoles. In the spherical coordinates, it is [6, Ch. 7]

$$\begin{aligned}\mathbf{G}(\mathbf{r},\mathbf{r}') = ik_0\sum_{n=1}^{\infty}\sum_{m=-n}^{n}\frac{1}{n(n+1)}\big[&\boldsymbol{\xi}_{nm1}(\mathbf{r})\boldsymbol{\psi}_{nm1}^\dagger(\mathbf{r}')\\ &+\boldsymbol{\xi}_{nm2}(\mathbf{r})\boldsymbol{\psi}_{nm2}^\dagger(\mathbf{r}')\big].\end{aligned} \quad (33)$$

The vector multipoles are defined as

$$\boldsymbol{\xi}_{nm1}(\mathbf{r}) = \nabla\times\left[\mathbf{r}h_n^{(1)}(k_0 r)Y_{nm}(\theta,\phi)\right] \quad (34a)$$

$$\boldsymbol{\xi}_{nm2}(\mathbf{r}) = \frac{1}{k_0}\nabla\times\nabla\times\left[\mathbf{r}h_n^{(1)}(k_0 r)Y_{nm}(\theta,\phi)\right] \quad (34b)$$

$$\boldsymbol{\psi}_{nm1}(\mathbf{r}) = \nabla\times\left[\mathbf{r}j_n(k_0 r)Y_{nm}(\theta,\phi)\right] \quad (34c)$$

$$\boldsymbol{\psi}_{nm2}(\mathbf{r}) = \frac{1}{k_0}\nabla\times\nabla\times\left[\mathbf{r}j_n(k_0 r)Y_{nm}(\theta,\phi)\right] \quad (34d)$$

where $h_n^{(1)}(\cdot)$ is the spherical Hankel function of the first kind, $Y_{nm}(\cdot,\cdot)$ is the spherical harmonic function, and $j_n(\cdot)$ is the spherical Bessel function. The $\boldsymbol{\xi}_{nml}(\mathbf{r})$'s are orthogonal on any spherical surface and $\boldsymbol{\psi}_{nml}(\mathbf{r})$'s are orthogonal in any spherical region. Suppose the antenna array is enclosed in a sphere of radius R. Then, the spectral elements defined in (28) are given by

$$\mathbf{u}_{nml}(\mathbf{r}) = \frac{\boldsymbol{\xi}_{nml}(\mathbf{r})}{\sqrt{\int|\boldsymbol{\xi}_{nml}(R_s\hat{\boldsymbol{\kappa}})|^2\,d\Omega}}$$

$$\mathbf{v}_{nml}(\mathbf{r}) = \frac{\boldsymbol{\psi}_{nml}^\dagger(\mathbf{r}')}{\sqrt{\int_{r\le R}|\boldsymbol{\psi}_{nml}(\mathbf{r})|^2\,d\mathbf{r}}}$$

$$\sigma_{nml} = \frac{\sqrt{\int|\boldsymbol{\xi}_{nml}(R_s\hat{\boldsymbol{\kappa}})|^2\,d\Omega}\sqrt{\int_{r\le R}|\boldsymbol{\psi}_{nml}(\mathbf{r})|^2\,d\mathbf{r}}}{n(n+1)}.$$

In Appendix C, we derive the singular values, and express them in terms of k_0R_s and k_0R

$$\begin{aligned}\sigma_{nm1}^2 = \frac{R^3}{2}|h_n^{(1)}(k_0R_s)|^2\Big[&j_{n-1}^2(k_0R)+j_n^2(k_0R)\\ &-\frac{2n+1}{k_0R}j_{n-1}(k_0R)j_n(k_0R)\Big]\end{aligned} \quad (35a)$$

$$\begin{aligned}\sigma_{nm2}^2 = \frac{R^3}{2}\Big[&\frac{n+1}{2n+1}\left|h_{n-1}^{(1)}(k_0R_s)\right|^2\\ &+\frac{n}{2n+1}\left|h_{n+1}^{(1)}(k_0R_s)\right|^2\Big]\\ \cdot\Big\{&\frac{n+1}{2n+1}\Big[j_{n-2}^2(k_0R)+j_{n-1}^2(k_0R)\\ &-\frac{2n-1}{k_0R}j_{n-2}(k_0R)j_{n-1}(k_0R)\Big]\\ &+\frac{n}{2n+1}\Big[j_n^2(k_0R)+j_{n+1}^2(k_0R)\\ &-\frac{2n+3}{k_0R}j_n(k_0R)j_{n+1}(k_0R)\Big]\Big\}.\end{aligned} \quad (35b)$$

The singular values depend on n but not m. When scatterers are in the far field of the antenna array, $k_0R_s \gg 1$. The spherical Hankel function can be approximated by

$$h_n^{(1)}(k_0R_s) = (-1)^{n+1}\frac{e^{ik_0R_s}}{k_0R_s}\left[1+\mathcal{O}\left(\frac{1}{k_0R_s}\right)\right].$$

The magnitude of the asymptotic term is independent of n and equals to $\frac{1}{k_0R_s}$. When $k_0R \gg 1$, $j_n(k_0R)\approx 0$ for $n > k_0R$. Hence, both σ_{nm1} and σ_{nm2} vanish when $n > k_0R$. As an example, Fig. 11 plots the distributions of σ_{nml}^2 for $R = 2\lambda$ and $R_s = 2R = 4\lambda$ where λ is a wavelength. Both σ_{nm1} and σ_{nm2} are small when $n > k_0R = 12.57$. Furthermore, the asymptotic term of $h_n^{(1)}(k_0R_s)$ provides a good approximation.

Asymptotically, the number of nonvanishing vector multipoles is $2(k_0R)^2$.

C. Degree-of-Freedom Gain

Volumetric Arrays in Fully-Scattered Channel: Here, we assume the volumetric array is a spherical array. The number of degrees of freedom therefore equals to the number of nonvanishing vector multipoles. When the source region is very small, only the lowest order multipoles can be used for information transmission. The lowest order multipoles correspond to $n = 1$ and the number of them is 6. Therefore, the degree-of-freedom gain for point sources is 6. When the source region increases, more multipoles can be used for information transmission and the number of them is asymptotically equal to $2(k_0R)^2$. A factor of 2 is due to the use of both magnetic multipole ($l = 1$) and electric multipole ($l = 2$), and it accounts for the degree-of-freedom gain from polarization. As $k_0 = 2\pi/\lambda$ and λ is a wavelength, the asymptotic number of degrees of freedom is $\min\left\{2\pi\sqrt[3]{36\pi}V_t^{2/3}, 2\pi\sqrt[3]{36\pi}V_r^{2/3}\right\} \approx \min\left\{30V_t^{2/3}, 30V_r^{2/3}\right\}$.

Volumetric Arrays in Azimuth-Scattered Channel: The rank of Σ_t and Σ_r equal to the respective number of nonvanishing multipoles in a fully-scattered channel. When the channel is less scattered, the number of degrees of freedom should be equal to or less than these ranks. It should then be equal to $\mathrm{E}_{\hat{\boldsymbol{\kappa}}}\left[\mathbf{U}^\dagger(R_s\hat{\boldsymbol{\kappa}})\mathbf{U}(R_s\hat{\boldsymbol{\kappa}})\right]$ where the columns of $\mathbf{U}^\dagger(R_s\hat{\boldsymbol{\kappa}})$ are $\mathbf{u}_{nml}(\mathbf{r})$'s for $n \leq \min\{k_0R_t, k_0R_r\} = n_{max}$, and R_t and R_r are the radius of the transmit and the receive source region respectively. The $\hat{\boldsymbol{\kappa}}$ is uniformly distributed on $\left\{(\theta,\phi) : 0 \leq \phi < 2\pi, \frac{\pi}{2} - \frac{\Delta}{2} \leq \theta < \frac{\pi}{2} + \frac{\Delta}{2}\right\}$.

The $\boldsymbol{\xi}_{nm1}(R_s\hat{\boldsymbol{\kappa}})$'s and $\boldsymbol{\xi}_{nm2}(R_s\hat{\boldsymbol{\kappa}})$'s are orthogonal over $0 \leq \phi < \pi$, $|\theta - \pi/2| \leq \Delta/2$ for different m only. That is, for the same m, the dimension of the functional space spanned by either $\boldsymbol{\xi}_{nm1}(R_s\hat{\boldsymbol{\kappa}})$'s or $\boldsymbol{\xi}_{nm2}(R_s\hat{\boldsymbol{\kappa}})$'s is 1. Consequently, the dimension of the space spanned by either $\mathbf{u}_{nm1}(R_s\hat{\boldsymbol{\kappa}})$'s or $\mathbf{u}_{nm2}(R_s\hat{\boldsymbol{\kappa}})$'s is $2n_{max} + 1$.

Next, we need to establish the orthogonality between the space spanned by $\mathbf{u}_{nm1}(R_s\hat{\boldsymbol{\kappa}})$'s and that by $\mathbf{u}_{nm2}(R_s\hat{\boldsymbol{\kappa}})$'s. It is suffice to show that $\boldsymbol{\xi}_{nm1}(R_s\hat{\boldsymbol{\kappa}})$'s and $\boldsymbol{\xi}_{nm2}(R_s\hat{\boldsymbol{\kappa}})$'s are orthogonal at $n = n_{max}$. From definition, it is also suffice to consider the orthogonality between $\nabla Y_{nm}(\theta,\phi) \times \mathbf{r}$ and $r\nabla Y_{nm}(\theta,\phi)$

$$\begin{aligned}&\int_0^{2\pi}\int_{\pi/2-\Delta/2}^{\pi/2+\Delta/2} r\nabla Y_{nm}(\theta,\phi)\\ &\quad\cdot\left[\nabla Y^*_{n'm'}(\theta,\phi)\times\mathbf{r}\right]\sin\theta\, d\theta d\phi\\ &= i2\pi m\delta_{mm'}\left[P_n^m\left(\frac{\Delta}{2}\right)P_{n'}^{m'}\left(\frac{\Delta}{2}\right) - P_n^m\left(-\frac{\Delta}{2}\right)P_{n'}^{m'}\left(-\frac{\Delta}{2}\right)\right]\end{aligned} \tag{36}$$

where $P_n^m(\cdot)$ is the associated Legendre function. At $n = n' = n_{max}$ and $m = m'$, the expression in the bracket is $O(\Delta^2)$. Asymptotically, $\mathbf{u}_{nml}(R_s\hat{\boldsymbol{\kappa}})$'s are orthogonal at $n = n_{max}$. Consequently, the number of degrees of freedom equals to $2(2n_{max} + 1) = \min\left\{2\pi\sqrt[3]{48/\pi V_t}, 2\pi\sqrt[3]{48/\pi V_r}\right\} \approx \min\left\{16V_t^{1/3}, 16V_r^{1/3}\right\}$.

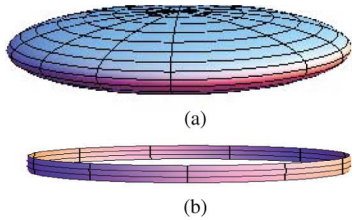

Fig. 12. (a) Oblate spheroid with large aspect ratio. (b) Surface of a portion of the oblate spheroid that includes the major equator.

TABLE II
SUMMARIZES THE ASYMPTOTIC NUMBER OF DEGREES OF FREEDOM FOR DIFFERENT TYPES OF ARRAY ELEMENTS AND ARRAY GEOMETRIES IN VARIOUS CHANNEL SCATTERING CONDITIONS

Channel	Array Element	Array Geometries			
		Point	Linear	Planar	Volumetric
Fully -Scattered	Vector	6	$12L$	$4\pi A$	$2\pi\sqrt[2/3]{6\pi^{1/2}V}$
	Scalar	1	$2L$	πA	$\pi\sqrt[2/3]{6\pi^{1/2}V}$
Azimuth -Scattered	Vector	6	$8L$	$8\sqrt{\pi A}$	$2\pi\sqrt[3]{48\pi^{-1}V}$
	Scalar	1	$2L$	$4\sqrt{\pi A}$	$\pi\sqrt[3]{48\pi^{-1}V}$

Planar Arrays in Azimuth-Scattered Channel: Here, we first argue that $\int_{\mathcal{V}_r}\mathbf{V}_r^\dagger(\mathbf{r})\mathbf{V}_r(\mathbf{r})\,d\mathbf{r}$ is greater than $\int_{\partial\mathcal{V}_r}\mathbf{V}_r^\dagger(\mathbf{r})\mathbf{V}_r(\mathbf{r})\,d\mathbf{r}$, and then argue that $\int_{\partial\mathcal{V}_r}\mathbf{V}_r^\dagger(\mathbf{r})\mathbf{V}_r(\mathbf{r})\,d\mathbf{r} = \mathrm{E}_{\hat{\boldsymbol{\kappa}}_r}\left[\mathbf{U}_r^\dagger(R_s\hat{\boldsymbol{\kappa}}_r)\mathbf{U}_r(R_s\hat{\boldsymbol{\kappa}}_r)\right]$. Hence, the number of degrees of freedom will be the same as in the case for volumetric array in azimuth-scattered channel.

We model the source region as a disk-like ellipsoid (oblate spheroid) with large aspect ratio as illustrated in Fig. 12(a). Now if we consider a portion of the ellipsoid that includes the major equator as shown in Fig. 12(b) and denote the corresponding surface at the receiver by $\partial\mathcal{V}_r$, the rank of $\int_{\partial\mathcal{V}_r}\mathbf{V}_r^\dagger(R_r\hat{\boldsymbol{\kappa}})\mathbf{V}_r(R_r\hat{\boldsymbol{\kappa}})\,d\hat{\boldsymbol{\kappa}}$ will be less than $\int_{\mathcal{V}_r}\mathbf{V}_r^\dagger(\mathbf{r})\mathbf{V}_r(\mathbf{r})\,d\mathbf{r}$.

Replacing Δ by the width of the ring in Fig. 12(b) and R_s by the radius of the source region, we can use the same argument for the volumetric array in azimuth-scattered channel and show that $\int_{\partial\mathcal{V}_r}\mathbf{V}_r^\dagger(\mathbf{r})\mathbf{V}_r(\mathbf{r})\,d\mathbf{r} = \mathrm{E}_{\hat{\boldsymbol{\kappa}}_r}\left[\mathbf{U}_r^\dagger(R_s\hat{\boldsymbol{\kappa}}_r)\mathbf{U}_r(R_s\hat{\boldsymbol{\kappa}}_r)\right]$. Hence, the number of degrees of freedom is $\min\left\{8\sqrt{\pi A_t}, 8\sqrt{\pi A_r}\right\} \approx \min\left\{14\sqrt{A_t}, 14\sqrt{A_r}\right\}$.

VII. CONCLUSION

In this paper, we use the sampling approach to derive the degree-of-freedom gain from using polarimetric antenna elements in conjunction with the multipole decomposition approach to derive the total number of degrees of freedom for different array geometries in various channel scattering conditions, as tabulated in Table II. The connection between the two approaches is that the point source used in the sampling approach corresponds to the set of lowest order multipoles ($n = 1$, $m = -1$, 0, 1, and $l = 1, 2$). The sampling approach uses the set of shifted lowest order multipoles to represent the signals while the vector multipole approach uses all multipoles to represent the signals. We use both approaches as neither of them gives exact results in all scenarios.

We show that the degree-of-freedom gain from using polarimetric antenna elements ranges from 2 to 6. From Physics, only 2 out of the 6 components of time-varying electric and magnetic field are independent at any point in space; that is, there are only two degrees of freedom from resolving the field directions. The extra factor in the degree-of-freedom gain for some array geometries is due to the use of polarimetric antenna elements in resolving the propagation directions of physical paths. For example, a scalar point source is not able to resolve any physical path but a point source with 6 co-located orthogonal dipoles is able to resolve physical paths to certain extent. Thus, there is a distinction between using polarimetric antenna elements to resolve the field directions and that to resolve the propagation directions of physical paths. Lower dimensional array geometries are not as effective in resolving the propagation directions, and therefore, the degree-of-freedom gain from using polarimetric antenna elements is higher.

Appendix A
Proof of (14) and (15)

For the fully-scattered channel, we consider the transformation matrices in (37) at the bottom of the page.

The covariance matrix of $\mathbf{U}_{r,k}^{\dagger}\mathbf{H}_{kl}^{a}\mathbf{U}_{t,l}$ is diagonal when

$$\alpha_{r,k}=\sqrt{\left(1-\frac{k}{L_r}\right)^2-\frac{1}{L_r}\left(1-\frac{k}{L_r}\right)+\frac{1}{3L_r^2}}$$
$$\beta_{r,k}=\sqrt{\left(1+\frac{k}{L_r}\right)^2+\frac{1}{L_r}\left(1+\frac{k}{L_r}\right)+\frac{1}{3L_r^2}}$$
$$\alpha_{t,l}=\sqrt{\left(1-\frac{l}{L_t}\right)^2-\frac{1}{L_t}\left(1-\frac{l}{L_t}\right)+\frac{1}{3L_t^2}}$$
$$\beta_{t,l}=\sqrt{\left(1+\frac{l}{L_t}\right)^2+\frac{1}{L_t}\left(1+\frac{l}{L_t}\right)+\frac{1}{3L_t^2}}.$$

Applying these pair of transformation matrices yields the result in (14).

For the azimuth-scattered channel, we consider the transformation matrices in (38) at the bottom of the next page to decorrelate the channel matrix. The diagonal elements of the covariance matrix of $\mathbf{U}_{r,k}^{\dagger}\mathbf{H}_{kl}^{a}\mathbf{U}_{t,l}$ vary as $O(\Delta)$ while the off-diagonal elements vary as $O(\Delta^3)$, when $\alpha_{r,k}$ and $\alpha_{t,l}$ satisfy (39) at the bottom of the next page. Applying those pair of transformation matrices yields the result in (15).

Appendix B
Proof of (20) and (22)

For the fully-scattered channel, we apply the following transformation matrices to decorrelate the channel matrix:

$$\mathbf{U}_{r,\mathbf{k}}=\begin{bmatrix}1&0&0&\gamma_{r,\mathbf{k}}&1&0\\0&\zeta_{r,\mathbf{k}}&\zeta_{r,\mathbf{k}}&0&0&-\zeta_{r,\mathbf{k}}\\0&\eta_{r,\mathbf{k}}&-\eta_{r,\mathbf{k}}&0&0&\eta_{r,\mathbf{k}}\\0&-\gamma_{r,\mathbf{k}}&-1&0&0&-1\\\zeta_{r,\mathbf{k}}&0&0&\zeta_{r,\mathbf{k}}&-\zeta_{r,\mathbf{k}}&0\\-\eta_{r,\mathbf{k}}&0&0&\eta_{r,\mathbf{k}}&\eta_{r,\mathbf{k}}&0\end{bmatrix}$$
$$\mathbf{U}_{t,\mathbf{l}}=\begin{bmatrix}1&0&0&\gamma_{t,\mathbf{l}}&1&0\\0&\zeta_{t,\mathbf{l}}&\zeta_{t,\mathbf{l}}&0&0&-\zeta_{t,\mathbf{l}}\\0&\eta_{t,\mathbf{l}}&-\eta_{t,\mathbf{l}}&0&0&\eta_{t,\mathbf{l}}\\0&-\gamma_{t,\mathbf{l}}&-1&0&0&-1\\\zeta_{t,\mathbf{l}}&0&0&\zeta_{t,\mathbf{l}}&-\zeta_{t,\mathbf{l}}&0\\-\eta_{t,\mathbf{l}}&0&0&\eta_{t,\mathbf{l}}&\eta_{t,\mathbf{l}}&0\end{bmatrix}$$

where

$$\zeta_{r,\mathbf{k}}=\sin\theta_{r,\mathbf{k}}\sin\phi_{r,\mathbf{k}}$$
$$\eta_{r,\mathbf{k}}=\sin\theta_{r,\mathbf{k}}\cos\phi_{r,\mathbf{k}}$$
$$\gamma_{r,\mathbf{k}}=\cos^2\phi_{r,\mathbf{k}}-\sin^2\phi_{r,\mathbf{k}}$$
$$\zeta_{t,\mathbf{l}}=\sin\theta_{t,\mathbf{l}}\sin\phi_{t,\mathbf{l}}$$
$$\eta_{t,\mathbf{l}}=\sin\theta_{t,\mathbf{l}}\cos\phi_{t,\mathbf{l}}$$
$$\gamma_{t,\mathbf{l}}=\cos^2\phi_{t,\mathbf{l}}-\sin^2\phi_{t,\mathbf{l}}.$$

Diagonal elements of the covariance of $\mathbf{U}_{r,\mathbf{k}}^{\dagger}\mathbf{H}_{\mathbf{kl}}^{a}\mathbf{U}_{t,\mathbf{l}}$ vary as $O\left(\frac{1}{A_tA_r}\right)$ while the off-diagonal elements vary as $O\left(\frac{1}{A_t^2A_r}\right)$

$$\mathbf{U}_{r,k}=\begin{bmatrix}1&0&0&0&0&0\\0&-\frac{\alpha_{r,k}-\beta_{r,k}}{\sqrt{2(\alpha_{r,k}^2+\beta_{r,k}^2)}}&0&0&0&\frac{\alpha_{r,k}+\beta_{r,k}}{\sqrt{2(\alpha_{r,k}^2+\beta_{r,k}^2)}}\\0&0&-\frac{\alpha_{r,k}-\beta_{r,k}}{\sqrt{2(\alpha_{r,k}^2+\beta_{r,k}^2)}}&0&\frac{\alpha_{r,k}+\beta_{r,k}}{\sqrt{2(\alpha_{r,k}^2+\beta_{r,k}^2)}}&0\\0&0&0&1&0&0\\0&0&\frac{\alpha_{r,k}+\beta_{r,k}}{\sqrt{2(\alpha_{r,k}^2+\beta_{r,k}^2)}}&0&-\frac{\alpha_{r,k}-\beta_{r,k}}{\sqrt{2(\alpha_{r,k}^2+\beta_{r,k}^2)}}&0\\0&-\frac{\alpha_{r,k}+\beta_{r,k}}{\sqrt{2(\alpha_{r,k}^2+\beta_{r,k}^2)}}&0&0&0&\frac{\alpha_{r,k}-\beta_{r,k}}{\sqrt{2(\alpha_{r,k}^2+\beta_{r,k}^2)}}\end{bmatrix}\tag{37a}$$

$$\mathbf{U}_{t,l}=\begin{bmatrix}1&0&0&0&0&0\\0&-\frac{\alpha_{t,l}-\beta_{t,l}}{\sqrt{2(\alpha_{t,l}^2+\beta_{t,l}^2)}}&0&0&0&\frac{\alpha_{t,l}+\beta_{t,l}}{\sqrt{2(\alpha_{t,l}^2+\beta_{t,l}^2)}}\\0&0&-\frac{\alpha_{t,l}-\beta_{t,l}}{\sqrt{2(\alpha_{t,l}^2+\beta_{t,l}^2)}}&0&\frac{\alpha_{t,l}+\beta_{t,l}}{\sqrt{2(\alpha_{t,l}^2+\beta_{t,l}^2)}}&0\\0&0&0&1&0&0\\0&0&\frac{\alpha_{t,l}+\beta_{t,l}}{\sqrt{2(\alpha_{t,l}^2+\beta_{t,l}^2)}}&0&-\frac{\alpha_{t,l}-\beta_{t,l}}{\sqrt{2(\alpha_{t,l}^2+\beta_{t,l}^2)}}&0\\0&-\frac{\alpha_{t,l}+\beta_{t,l}}{\sqrt{2(\alpha_{t,l}^2+\beta_{t,l}^2)}}&0&0&0&\frac{\alpha_{t,l}-\beta_{t,l}}{\sqrt{2(\alpha_{t,l}^2+\beta_{t,l}^2)}}\end{bmatrix}\tag{37b}$$

and $O\left(\frac{1}{A_t A_r^2}\right)$. For A_t and A_r large, the nonzero elements of $\mathbf{U}_{r,\mathbf{k}}^{\dagger}\mathbf{H}_{\mathbf{kl}}^{a}\mathbf{U}_{t,\mathbf{l}}$ are approximately independent. Its variance matrix is presented in (20).

For the azimuth-scattered channel, we apply the following transformation matrices to decorrelate the elements of the channel matrix:

$$\mathbf{U}_{r,\mathbf{k}} = \begin{bmatrix} 1 & 0 & 0 & \gamma_{r,\mathbf{k}} & 1 & 0 \\ 0 & \zeta_{r,\mathbf{k}} & \zeta_{r,\mathbf{k}} & 0 & 0 & -\zeta_{r,\mathbf{k}} \\ 0 & -\eta_{r,\mathbf{k}} & \eta_{r,\mathbf{k}} & 0 & 0 & \eta_{r,\mathbf{k}} \\ 0 & -1 & -\gamma_{r,\mathbf{k}} & 0 & 0 & -1 \\ \zeta_{r,\mathbf{k}} & 0 & 0 & \zeta_{r,\mathbf{k}} & -\zeta_{r,\mathbf{k}} & 0 \\ -\eta_{r,\mathbf{k}} & 0 & 0 & \eta_{r,\mathbf{k}} & \eta_{r,\mathbf{k}} & 0 \end{bmatrix}$$

$$\mathbf{U}_{t,\mathbf{l}} = \begin{bmatrix} 1 & 0 & 0 & \gamma_{t,\mathbf{l}} & 1 & 0 \\ 0 & \zeta_{t,\mathbf{l}} & \zeta_{t,\mathbf{l}} & 0 & 0 & -\zeta_{t,\mathbf{l}} \\ 0 & -\eta_{t,\mathbf{l}} & \eta_{t,\mathbf{l}} & 0 & 0 & \eta_{t,\mathbf{l}} \\ 0 & -1 & -\gamma_{t,\mathbf{l}} & 0 & 0 & -1 \\ \zeta_{t,\mathbf{l}} & 0 & 0 & \zeta_{t,\mathbf{l}} & -\zeta_{t,\mathbf{l}} & 0 \\ -\eta_{t,\mathbf{l}} & 0 & 0 & \eta_{t,\mathbf{l}} & \eta_{t,\mathbf{l}} & 0 \end{bmatrix}$$

where

$$\begin{aligned} \zeta_{r,\mathbf{k}} &= \sin\phi_{r,\mathbf{k}} \\ \eta_{r,\mathbf{k}} &= \cos\phi_{r,\mathbf{k}} \\ \gamma_{r,\mathbf{k}} &= \cos^2\phi_{r,\mathbf{k}} - \sin^2\phi_{r,\mathbf{k}} \\ \zeta_{t,\mathbf{l}} &= \sin\phi_{t,\mathbf{l}} \\ \eta_{t,\mathbf{l}} &= \cos\phi_{t,\mathbf{l}} \\ \gamma_{t,\mathbf{l}} &= \cos^2\phi_{t,\mathbf{l}} - \sin^2\phi_{t,\mathbf{l}}. \end{aligned}$$

For $\frac{\Delta}{\sqrt{A_t}}$, $\frac{\Delta}{\sqrt{A_r}}$ small, elements of $\mathbf{U}_{r,\mathbf{k}}^{\dagger}\mathbf{H}_{\mathbf{kl}}^{a}\mathbf{U}_{t,\mathbf{l}}$ are approximately independent. The variance matrix is presented in (22).

Appendix C
Proof of (35)

From definition

$$\boldsymbol{\xi}_{nm1}(\mathbf{r}) = \nabla Y_{nm}(\theta,\phi) \times \mathbf{r} h_n^{(1)}(k_0 r). \tag{40}$$

Using (9.120) in [9], we obtain

$$\begin{aligned} &\int \mathbf{r}\times\nabla Y_{nm}(\theta,\phi)\cdot\mathbf{r}\times\nabla Y_{n'm'}^{*}(\theta,\phi)d\Omega \\ &= \int r\nabla Y_{nm}(\theta,\phi)\cdot r\nabla Y_{n'm'}^{*}(\theta,\phi)\,d\Omega \\ &= n(n+1)\delta_{nn'}\delta_{mm'}. \end{aligned}$$

This yields

$$\int |\boldsymbol{\xi}_{nm1}(R_s,\theta,\phi)|^2\,d\Omega = n(n+1)|h_n^{(1)}(k_0R_s)|^2. \tag{41}$$

To find the correspondence for $\boldsymbol{\xi}_{nm2}(R_s,\theta,\phi)$, it requires some work that is not in standard electromagnetic textbooks. We apply (3.12c) in [10] to obtain

$$\begin{aligned} \boldsymbol{\xi}_{nm2}(\mathbf{r}) &= n(n+1)\frac{h_n^{(1)}(k_0r)}{k_0r}\hat{\mathbf{r}}Y_{nm}(\theta,\phi) \\ &\quad + \frac{1}{k_0r}\frac{d}{dr}\left[rh_n^{(1)}(k_0r)\right]r\nabla Y_{nm}(\theta,\phi) \\ &= n(n+1)\frac{h_n^{(1)}(k_0r)}{k_0r}\hat{\mathbf{r}}Y_{nm}(\theta,\phi) + \Big[h_{n-1}^{(1)}(k_0r) \end{aligned} \tag{42}$$

$$\mathbf{U}_{r,k} = \begin{bmatrix} 0 & \frac{1}{\sqrt{1+\alpha_{r,k}^2}} & 0 & 0 & 0 & \frac{1}{\sqrt{1+\alpha_{r,k}^2}} \\ 0 & 0 & 1 & 0 & 0 & 0 \\ 0 & 0 & 0 & \frac{\alpha_{r,k}}{\sqrt{1+\alpha_{r,k}^2}} & -\frac{\alpha_{r,k}}{\sqrt{1+\alpha_{r,k}^2}} & 0 \\ 0 & 0 & 0 & \frac{1}{\sqrt{1+\alpha_{r,k}^2}} & \frac{1}{\sqrt{1+\alpha_{r,k}^2}} & 0 \\ 1 & 0 & 0 & 0 & 0 & 0 \\ 0 & -\frac{\alpha_{r,k}}{\sqrt{1+\alpha_{r,k}^2}} & 0 & 0 & 0 & \frac{\alpha_{r,k}}{\sqrt{1+\alpha_{r,k}^2}} \end{bmatrix} \tag{38a}$$

$$\mathbf{U}_{t,l} = \begin{bmatrix} 0 & \frac{1}{\sqrt{1+\alpha_{t,l}^2}} & 0 & 0 & 0 & \frac{1}{\sqrt{1+\alpha_{t,l}^2}} \\ 0 & 0 & 1 & 0 & 0 & 0 \\ 0 & 0 & 0 & \frac{\alpha_{t,l}}{\sqrt{1+\alpha_{t,l}^2}} & -\frac{\alpha_{t,l}}{\sqrt{1+\alpha_{t,l}^2}} & 0 \\ 0 & 0 & 0 & \frac{1}{\sqrt{1+\alpha_{t,l}^2}} & \frac{1}{\sqrt{1+\alpha_{t,l}^2}} & 0 \\ 1 & 0 & 0 & 0 & 0 & 0 \\ 0 & -\frac{\alpha_{t,l}}{\sqrt{1+\alpha_{t,l}^2}} & 0 & 0 & 0 & \frac{\alpha_{t,l}}{\sqrt{1+\alpha_{t,l}^2}} \end{bmatrix} \tag{38b}$$

$$\alpha_{r,k} = \operatorname{sgn}(k)\sqrt{\frac{2\left(\cos^{-1}\frac{k}{L_r} - \cos^{-1}\frac{k+1}{L_r}\right)}{\frac{k}{L_r}\sqrt{1-\frac{k^2}{L_r^2}} - \frac{k+1}{L_r}\sqrt{1-\frac{(k+1)^2}{L_r^2}} + \cos^{-1}\frac{k}{L_r} - \cos^{-1}\frac{k+1}{L_r}}} \tag{39a}$$

$$\alpha_{t,l} = \operatorname{sgn}(l)\sqrt{\frac{2\left(\cos^{-1}\frac{l}{L_t} - \cos^{-1}\frac{l+1}{L_t}\right)}{\frac{l}{L_t}\sqrt{1-\frac{l^2}{L_t^2}} - \frac{l+1}{L_t}\sqrt{1-\frac{(l+1)^2}{L_t^2}} + \cos^{-1}\frac{l}{L_t} - \cos^{-1}\frac{l+1}{L_t}}} \tag{39b}$$

$$- n\frac{h_n^{(1)}(k_0 r)}{k_0 r}\Big] r\nabla Y_{nm}(\theta,\phi). \tag{43}$$

As

$$\int \hat{\mathbf{r}} Y_{nm}(\theta,\phi)\cdot\hat{\mathbf{r}} Y^*_{n'm'}(\theta,\phi)\,d\Omega = \delta_{nn'}\delta_{mm'}$$
$$\int \hat{\mathbf{r}} Y_{nm}(\theta,\phi)\cdot r\nabla Y^*_{n'm'}(\theta,\phi)\,d\Omega = 0$$

we obtain

$$\int |\boldsymbol{\xi}_{nm2}(R_s,\theta,\phi)|^2\,d\Omega = \frac{n(n+1)^2}{2n+1}\left|h_{n-1}^{(1)}(k_0R_s)\right|^2 + \frac{n^2(n+1)}{2n+1}\left|h_{n+1}^{(1)}(k_0R_s)\right|^2. \tag{44}$$

Replacing $h_n^{(1)}(k_0R_s)$ with $j_n(k_0R_s)$ yields the integration of the angular part of $|\boldsymbol{\psi}_{nml}(\mathbf{r})|^2$. Thus, we obtain

$$\begin{aligned}\int_{r\le R} |\boldsymbol{\psi}_{nm1}(\mathbf{r})|^2\,d\mathbf{r} &= \int_0^R n(n+1)j_n^2(k_0r)r^2\,dr \\ &= \frac{n(n+1)R^3}{2}\Big[j_{n-1}^2(k_0R) + j_n^2(k_0R) \\ &\quad - \frac{2n+1}{k_0R}j_{n-1}(k_0R)j_n(k_0R)\Big]\end{aligned} \tag{45}$$

and

$$\begin{aligned}\int_{r\le R} |\boldsymbol{\psi}_{nm2}(\mathbf{r})|^2\,d\mathbf{r} &= \frac{n(n+1)^2R^3}{2(2n+1)}\Big[j_{n-2}^2(k_0R) + j_{n-1}^2(k_0R) \\ &\quad - \frac{2n-1}{k_0R}j_{n-2}(k_0R)j_{n-1}(k_0R)\Big] \\ &\quad + \frac{n^2(n+1)R^3}{2(2n+1)}\Big[j_n^2(k_0R) + j_{n+1}^2(k_0R) \\ &\quad - \frac{2n+3}{k_0R}j_n(k_0R)j_{n+1}(k_0R)\Big].\end{aligned} \tag{46}$$

As a whole, we have

$$\begin{aligned}\sigma_{nm1}^2 &= \frac{R^3}{2}|h_n^{(1)}(k_0R_s)|^2\Big[j_{n-1}^2(k_0R) + j_n^2(k_0R) \\ &\quad - \frac{2n+1}{k_0R}j_{n-1}(k_0R)j_n(k_0R)\Big] \\ \sigma_{nm2}^2 &= \frac{R^3}{2}\Big[\frac{n+1}{2n+1}\left|h_{n-1}^{(1)}(k_0R_s)\right|^2 \\ &\quad + \frac{n}{2n+1}\left|h_{n+1}^{(1)}(k_0R_s)\right|^2\Big] \\ &\quad \cdot\Big\{\frac{n+1}{2n+1}\Big[j_{n-2}^2(k_0R) + j_{n-1}^2(k_0R) \\ &\quad - \frac{2n-1}{k_0R}j_{n-2}(k_0R)j_{n-1}(k_0R)\Big] \\ &\quad + \frac{n}{2n+1}\Big[j_n^2(k_0R) + j_{n+1}^2(k_0R) \\ &\quad - \frac{2n+3}{k_0R}j_n(k_0R)j_{n+1}(k_0R)\Big]\Big\}.\end{aligned}$$

ACKNOWLEDGMENT

The authors would like to thank Professor Weng-Cho Chew of the University of Illinois at Urbana-Champaign for the useful discussions during the initial development of this work.

REFERENCES

[1] M. R. Andrews, P. P. Mitra, and R. deCarvalho, "Tripling the capacity of wireless communications using electromagnetic polarization," *Nature*, vol. 409, pp. 316–318, Jan. 2001.

[2] T. Svantesson, M. A. Jensen, and J. W. Wallace, "Analysis of electromagnetic field polarizations in multiantenna systems," *IEEE Trans. Wireless Commun.*, vol. 3, no. 2, pp. 641–646, Mar. 2004.

[3] M. Gustafsson and S. Nordebo, "Characterization of MIMO antenna using spherical vector waves," *IEEE Trans. Antennas Propagat.*, vol. 54, no. 9, pp. 2679–2682, Sep. 2006.

[4] T. L. Marzetta, "Fundamental limitations on the capacity of wireless links that use polarimetric antenna arrays," in *Proc. IEEE Int. Symp. Information Theory*, Jul. 2002, pp. 51–51.

[5] A. S. Y. Poon, R. W. Brodersen, and D. N. C. Tse, "Degrees of freedom in multiple-antenna channels: A signal space approach," *IEEE Trans. Inf. Theory*, vol. 51, no. 2, pp. 523–536, Feb. 2005.

[6] W. C. Chew, *Waves and Fields in Inhomogeneous Media*. New York: IEEE, 1995.

[7] W. C. Jakes, *Microwave Mobile Communications*. Hoboken, NJ: Wiley, 1974.

[8] D. P. Petersen and D. Middleton, "Sampling and reconstruction of wave-number-limited functions in n-dimensional Euclidean spaces," *Inf. Control*, no. 5, pp. 279–323, 1962.

[9] J. D. Jackson, *Classical Electrodynamics*, 3rd ed. Hoboken, NJ: Wiley, 1998.

[10] R. G. Barrera, G. A. Estévez, and J. Giraldo, "Vector spherical harmonics and their application to magnetostatics," *Eur. J. Phys.*, vol. 6, pp. 287–294, 1985.

Ada S. Y. Poon (S'98–M'04–SM'10) received the B.Eng. and M.Phil. degrees in Electrical and Electronic Engineering from the University of Hong Kong in 1996 and 1997 respectively, and received the M.S. and Ph.D. degrees in Electrical Engineering and Computer Sciences from the University of California at Berkeley in 1999 and 2004 respectively. In 2004, she was a senior research scientist at Intel Corporation, Santa Clara, CA. In 2005, she was a senior technical fellow at SiBeam, Inc., Fremont, CA. In 2006–2007, she was an assistant professor at the Department of Electrical and Computer Engineering in the University of Illinois at Urbana-Champaign. Since 2008, she has been at the Department of Electrical Engineering in Stanford University, where she is currently an assistant professor.

Her current research interests focus on the applications of electrical engineering to advance surgical instruments, and *in vivo* diagnostics and therapeutic treatments.

David N. C. Tse (S'91–M'96–SM'07–F'11) received the B.A.Sc. degree in systems design engineering from the University of Waterloo, Canada in 1889 and the M.S. and Ph.D. degrees in Electrical Engineering from the Massachusetts Institute of Technology, Cambridge in 1991 and 1994 respectively.

From 1994 to 1995, he was a postdoctoral member of technical staff at A.T. & T. Bell Laboratories. Since 1995, he has been at the Department of Electrical Engineering and Computer Sciences in the University of California at Berkeley, where he is currently a Professor. He received a 1967 NSERC 4-year graduate fellowship from the government of Canada in 1989, a NSF CAREER award in 1998, the Best Paper Awards at the Infocom 1998 and Infocom 2001 conferences, the Erlang Prize in 2000 from the INFORMS Applied Probability Society, the IEEE Communications and Information Theory Society Joint Paper Award in 2001, and the Information Theory Society Paper Award in 2003. He was the Technical Program co-chair of the International Symposium on Information Theory in 2004, and was an Associate Editor of the IEEE TRANSACTIONS ON INFORMATION THEORY from 2001 to 2003. He is a coauthor, with Pramod Viswanath, of the text *Fundamentals of Wireless Communication*. His research interests are in information theory, wireless communications, and networking.